

CPEB1-dependent disruption of the mRNA translation program in oocytes during maternal aging

Received: 12 April 2022

Accepted: 11 January 2023

Published online: 26 January 2023

 Check for updatesNozomi Takahashi^{1,2,3}, Federica Franciosi^{1,2,3,4}, Enrico Maria Daldello^{1,2,3,5}, Xuan G. Luong^{1,2,3}, Peter Althoff^{1,2,3}, Xiaotian Wang^{1,2,3} & Marco Conti^{1,2,3} ✉

The molecular causes of deteriorating oocyte quality during aging are poorly defined. Since oocyte developmental competence relies on post-transcriptional regulations, we tested whether defective mRNA translation contributes to this decline in quality. Disruption in ribosome loading on maternal transcripts is present in old oocytes. Using a candidate approach, we detect altered translation of 3'-UTR-reporters and altered poly(A) length of the endogenous mRNAs. mRNA polyadenylation depends on the cytoplasmic polyadenylation binding protein 1 (CPEB1). *Cpeb1* mRNA translation and protein levels are decreased in old oocytes. This decrease causes de-repression of *Ccnb1* translation in quiescent oocytes, premature CDK1 activation, and accelerated reentry into meiosis. De-repression of *Ccnb1* is corrected by *Cpeb1* mRNA injection in old oocytes. Oocyte-specific *Cpeb1* haploinsufficiency in young oocytes recapitulates all the translation phenotypes of old oocytes. These findings demonstrate that a dysfunction in the oocyte translation program is associated with the decline in oocyte quality during aging.

Loss of homeostasis and decreased ability to respond to metabolic challenges is a hallmark of cellular aging¹. However, the aging-related decline in cellular functions does not progress in a synchronous fashion in all cells and tissues of the body. One striking example is the ovary, where an age-related decrease in the number and quality of oocytes causes a decline in fertility that precedes other aging-induced loss of function². Although aging patients can carry a pregnancy to term with oocyte donation^{3,4}, the decrease in oocyte developmental competence is a major hurdle in the Assisted Reproductive Technologies (ARTs) setting. The decline in oocyte quality has been imputed to several causes, with an increased incidence of aneuploidy of the egg or the embryo and genomic instability perhaps caused by epigenetic errors or metabolic insults being the most widely reported⁵⁻⁷.

The oocyte's ability to develop as an embryo and to support pregnancy through a live birth relies on a complex set of developmental processes, including the coordinated acquisition of gamete meiotic and cytoplasmic competence^{8,9}. Less clear is the role of cytoplasmic competence in the decline in fertility with age. Cytoplasmic maturation includes the assembly of the molecular machinery necessary for the completion of meiosis, for reprogramming of organelle morphology and their redistribution within the oocyte. It should be underscored that upon fertilization the oocyte cytoplasm is transferred to the zygote. Therefore, the transcriptional activation of the embryo genome takes place in this maternal environment⁹⁻¹¹. Several observations in the ART practice point to defective cytoplasmic competence as a cause of the decrease in embryo fitness to develop and implant¹².

¹Center for Reproductive Sciences, University of California, San Francisco, CA 94143, USA. ²USA Eli and Edythe Broad Center of Regeneration Medicine and Stem Cell Research, University of California, San Francisco, CA 94143, USA. ³Department of Obstetrics and Gynecology and Reproductive Sciences, University of California, San Francisco, CA 94143, USA. ⁴Present address: Reproductive and Developmental Biology Lab, Department of Veterinary Medicine and Animal Science, Università degli Studi di Milano, 20133 Milan, Italy. ⁵Present address: Sorbonne Université, CNRS, Laboratoire de Biologie du Développement—Institut de Biologie Paris Seine, LBD-IBPS, Paris, France. ✉ e-mail: Marco.Conti@ucsf.edu

Oocyte maturation is the last step of oogenesis. In a span of several hours, a Prophase I arrested oocyte (also called germinal vesicle (GV) stage oocyte) re-enters meiosis in response to the luteinizing hormone (LH) surge, undergoes nuclear envelop breakdown (NEBD) or germinal vesicle breakdown, GVBD), completes the first meiotic division, and finally arrests at the MII stage of meiosis. MII oocytes are then ovulated and ready to be fertilized. Removal of a GV-arrested, fully grown oocyte, from the antral follicle initiates a cascade of events called spontaneous maturation that recapitulates maturation to the MII stage in vitro. During these final stages of oocyte maturation, the synthesis of proteins critical for developmental competence relies on a program of timed translation of long-lived mRNAs that have been synthesized earlier during oocyte growth^{13–15}. Thus, gene expression in oocytes is controlled by translation in the cytoplasm rather than via transcription in the nucleus. This property, shared by the gametes of most species¹⁶, clearly indicates that the translational program executed at the oocyte-to-zygote transition is integral to the acquisition of developmental competence. We have provided evidence that defects in the translation program are associated with compromised developmental competence in the mouse^{17–19}. One central mechanism of translation regulation of maternal mRNAs relies on the dynamic modulation of the poly(A) tail associated with the mRNA 3'-untranslated region (3'-UTR)²⁰. A major regulator of polyadenylation is the cytoplasmic polyadenylation element binding protein 1 (CPEB1)^{20,21}. This RNA-binding protein modulates the translation of mRNAs containing the cytoplasmic polyadenylation element (CPE). Our genome-wide analysis revealed a global switch in maternal mRNA translation coinciding with oocyte reentry into the meiotic cell cycle and the crucial role of CPEB1 in directing this switch¹⁵.

Here, we propose the hypothesis that a defective execution of the maternal mRNA translation program during oocyte maturation also leads to the compromised developmental competence observed during maternal aging. In contrast to the numerous transcriptomic studies published on oocyte aging^{22–25}, scarce information is available as to whether defects in the translation program contribute to the age-related decline in oocyte quality^{26,27}. Using a RiboTag Immunoprecipitation (IP) strategy²⁸ in mouse oocytes²⁹, we have compared ribosome loading in MII oocytes from young and old mice. We provide evidence for defects in the mRNA translation program in oocytes derived from old female mice, a disruption that is associated with decreased CPEB1 function. In turn, these defects likely contribute to the decline in developmental competence and age-associated infertility.

Results

RiboTag IP/RNA-Seq reveals a disruption in the pattern of mRNA translation during maternal aging

Previous studies have examined the transcriptome in quiescent (GV) and matured (MII) oocytes from young and old mice (dataset GDS3295)²⁴. A conclusion of this study is that a significant number of transcripts are decreased in aging oocytes²⁴. However, our re-analysis of these datasets also shows that levels of 2109 transcripts increase significantly from GV to MII in young oocytes (Supplementary Fig. 1a). Mouse oocyte maturation occurs in the virtual absence of transcription, as fully matured oocytes show highly condensed chromatin, and RNA synthesis is at background level¹³. Given this genome-wide transcriptional silencing, mRNA levels in maturing oocytes should only remain stable or decrease, the decrease being caused by destabilization/degradation^{15,30}. Therefore, we hypothesize that the widespread increase in transcript levels is due to a bias towards polyadenylated mRNA species introduced during cDNA synthesis using oligo(-dT) primers, a possibility also raised in the original publication²⁴. The apparent increase in mRNA levels would then reflect differences in polyadenylation/translation rather than mRNA steady-state levels, a possibility also proposed in other oocyte transcriptomic studies^{31,32}.

Indeed, a comparison of apparently increased transcripts in GDS3295²⁴ with our datasets probing ribosome loading¹⁴ show considerable overlap with activated mRNAs (Supplementary Fig. 1a–c). Moreover, direct measurement of poly(A) length and efficiency of oligo(-dT) priming confirms such a correlation (Supplementary Fig. 2). The apparent differences between young and old oocytes found in the aging transcriptome may, therefore, indicate defective polyadenylation (Supplementary Fig. 1d) rather than altered transcript levels.

To directly assess this possibility, we compared transcriptome and translome in MII oocytes from young (1 month) and old (12–15 months) mice using the RiboTag IP/RNA-Seq ribosome-loading strategy²⁹ and random priming library preparation. Properties of the oocyte samples are reported in Supplementary Fig. 3a–e, and data quality control analysis of the RNA-Seq data is reported in Supplementary Fig. 4a, b. With the exception of 47 mRNAs, total mRNA levels (input) did not differ significantly between young and old MII oocytes (FDR < 0.05, Fig. 1a). Conversely, ribosome loading was significantly decreased for 254 mRNAs and increased for 38 mRNAs in old oocytes compared with young oocytes (FDR < 0.05, Fig. 1b). The list of input and HA genes significantly different are provided in Supplementary Data 1 and 2. Relaxing the statistical stringency to FDR < 0.1 increased the number of mRNAs with significantly altered ribosome loading to 726. Gene ontology analysis of the decreased and increased mRNAs showed enrichment in terms that include “mitochondrion” and “nucleus” (Fig. 1c). Further mining of the data showed that the translation efficiency for a significant number of mRNAs encoding mitochondrial ribosomal proteins is disrupted in old oocytes compared to young, although input levels are comparable (Fig. 1d). Alteration in mitochondrial ribosomal protein mRNA translation has been reported for several tissues of an aging organism^{33–35}, and mitochondrion dysfunction during aging is well-established³⁶ including for the oocytes³⁷. Thus, our RiboTag IP/RNA-Seq analysis detected changes shown to be associated with aging and provided an indication that disruption of mRNA translation is present in old oocytes.

3'-UTRs of affected transcripts drive defective mRNA translation during maternal aging

For a better characterization of the defects in translation associated with maternal aging, we used a candidate gene approach. To capture the broad changes suggested in the previous aging transcriptome and detected by RNA-Seq, we included the following genes among the candidates analyzed. TPX2 was used as a control, not being significantly different in the aging transcriptome and in our RNA-Seq. NLRP5 (MATER), a component of the subcortical maternal complex³⁸ for which an increase was detected in the RNA-Seq and in the aging transcriptome, was used as a prototypic upregulated mRNA during aging. *Golph3*, *Il7*, and *Thumpd1* were used as representative down-regulated mRNAs, with a decrease detected in one or both datasets. GOLPH3 is a component of the Golgi apparatus, an organelle undergoing major restructuring during oocyte maturation³⁹. THUMPDI encodes an RNA-binding protein involved in the acetylation of RNA and ribosome biogenesis⁴⁰. We have previously shown that translation of *IL7* mRNA and protein secretion increase during oocyte maturation, and its accumulation in follicular fluid (FF) of in vitro fertilization (IVF) patients correlates with oocyte maturation and egg quality⁴¹. Given this correlation between *IL7* secretion and oocyte quality, we included this candidate because it is significantly decreased in the aging transcriptome, even though no changes in translation were detected for this mRNA in the RNA-Seq dataset.

Reporters were generated by fusing the enhanced YFP fluorescent protein to the 3'-UTR of *Tpx2*, *Nlrp5*, *Golph3*, *Il7* or *Thumpd1* mRNAs. After in vitro translation, these construct mRNAs were injected together with an mCherry mRNA in denuded oocytes from young and old mice, and the rate of translation was monitored by time-lapse microscopy throughout maturation (Fig. 2a). Used as a

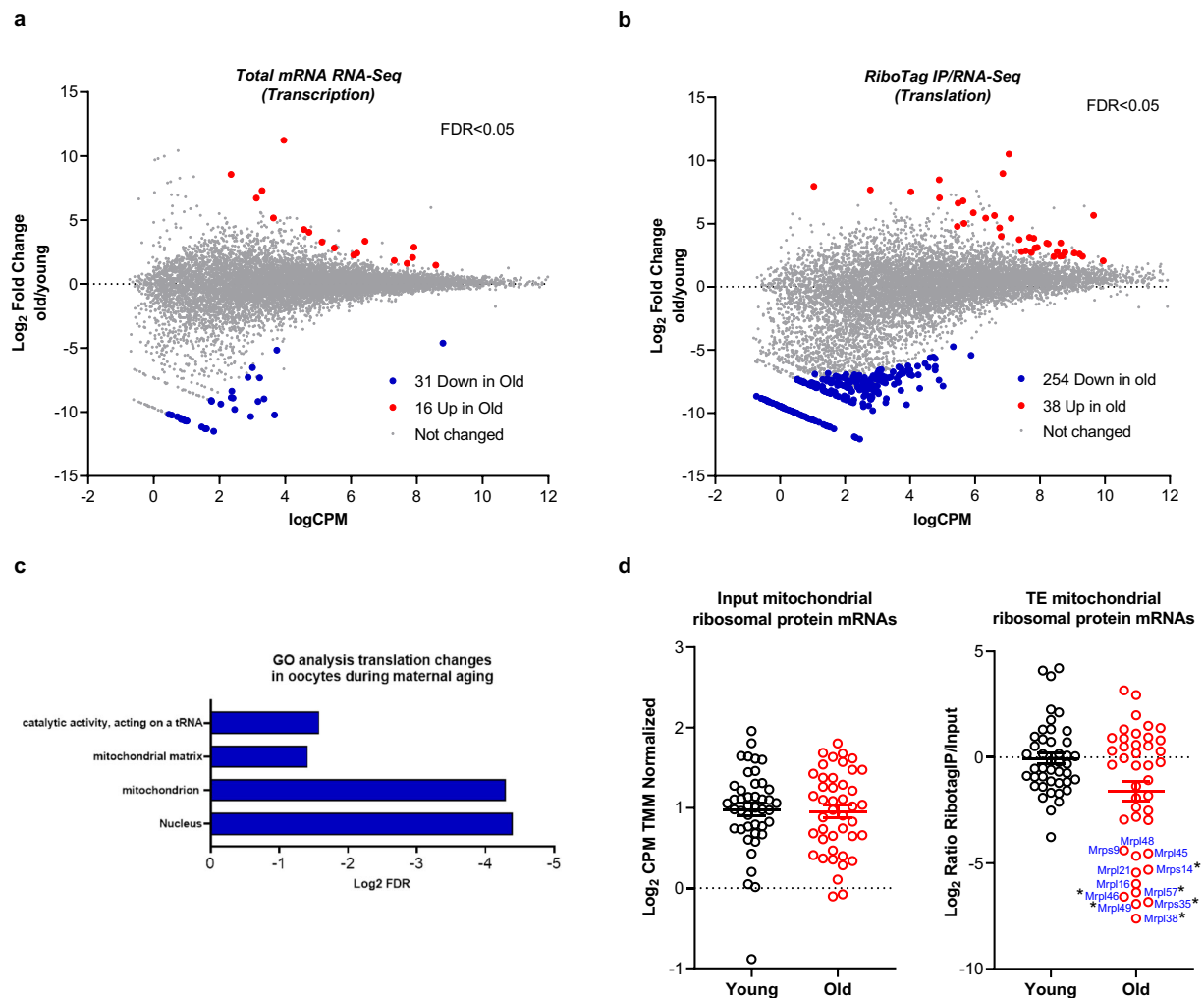


Fig. 1 | Differences in transcriptome and translome in young and old MII oocytes. MII oocytes were collected from young and old *RiboTag^{+/+};Zp3-Cre* mice and RiboTag IP followed by RNA-Seq was performed as described in “Methods”. Two biological independent samples are used. **a**, **b** MA-plot of gene expression changes for total transcripts (**a**) and ribosome loading on transcripts (**b**) are reported. The log₂ fold changes for young vs old oocytes is plotted on the y axis and the log₁₀ of the average counts per million reads (CPM) is shown on the x axis. Each gene is represented by a dot. Genes with FDR < 0.05 are shown in red (upregulated) or blue (downregulated). **c** Gene ontology analysis of mRNAs

whose translation is significantly (FDR < 0.1) different between young and old oocytes, including both upregulated and downregulated transcripts. Note the highly significant enrichment in mitochondrion term. **d** Comparison of levels of mRNAs coding for mitochondrial ribosomal protein and their translation efficiency (TE) in young and old oocytes. The log₂ of the average CPM is plotted on the y axis. The bar represents mean ± SEM. A subset of mRNAs coding for mitochondrial ribosomal proteins is poorly translated in aging oocytes. *FDR < 0.05. Source data are provided as a Source Data file.

loading control, mCherry signal was comparable for all reporters between young and old oocytes (Supplementary Fig. 5). Translation pattern can be divided into three main categories. In addition to a pattern of constitutive translation, mRNAs undergo decreased translation during oocyte maturation as *Nlrp5*, while activated translation is observed for another group, including *Il7*, *Thumpd1*, and *Golph3*. Supplementary Fig. 6 highlights two opposing patterns of ribosome loading during maturation and YFP accumulation in oocytes maintained in GV or during in vitro maturation. *Nlrp5* translation in young oocytes progressively decreased to a plateau (Supplementary Fig. 6c and Fig. 2d), reflecting repression of translation, a finding consistent with ribosome loading (Supplementary Figs. 1c and 6a). However, in old oocytes the rate of translation of this reporter was initially comparable in the two groups but, with time, it did not plateau as in young oocytes (Fig. 2d). This suggests that translation in old oocytes is not correctly repressed, a finding consistent with the data from the aging transcriptome and ribosome loading. The YFP accumulation driven by the *Golph3*, *Il7*, and *Thumpd1* 3'-UTR underwent activation about 3 h after GVBD and continued to increase

thereafter (Supplementary Fig. 6d and Fig. 2f, h, j), findings again consistent with the ribosome loading (see supplementary Figs. 1c and 6b). However, a decreased accumulation of the reporter was detected in old oocytes for all three 3'-UTRs. To quantify differences in reporter translation, the rate of accumulation was calculated for each injected oocyte using curve fitting⁴². Using this approach, the translation rate of *Golph3*, *Il7*, and *Thumpd1* is significantly decreased in old oocytes compared to young (Fig. 2g, i, k), while the translation of *Nlrp5* is significantly increased in old oocytes (Fig. 2e). No difference in translation was detected in *Tpx2* (Fig. 2b, c), confirming that altered translation is not a generalized phenomenon. Therefore, the increased, decreased, or unchanged accumulation of these reporters is consistent with the apparent changes in the aging transcriptome and with our ribosome loading data.

Given our previous finding that translation in oocytes is sensitive to the presence of surrounding cumulus cells¹⁷, we then tested whether translation under these more physiological conditions were altered in old oocytes. When oocytes are still surrounded by the cumulus cells, they are difficult to monitor via time-lapse microscopy due to

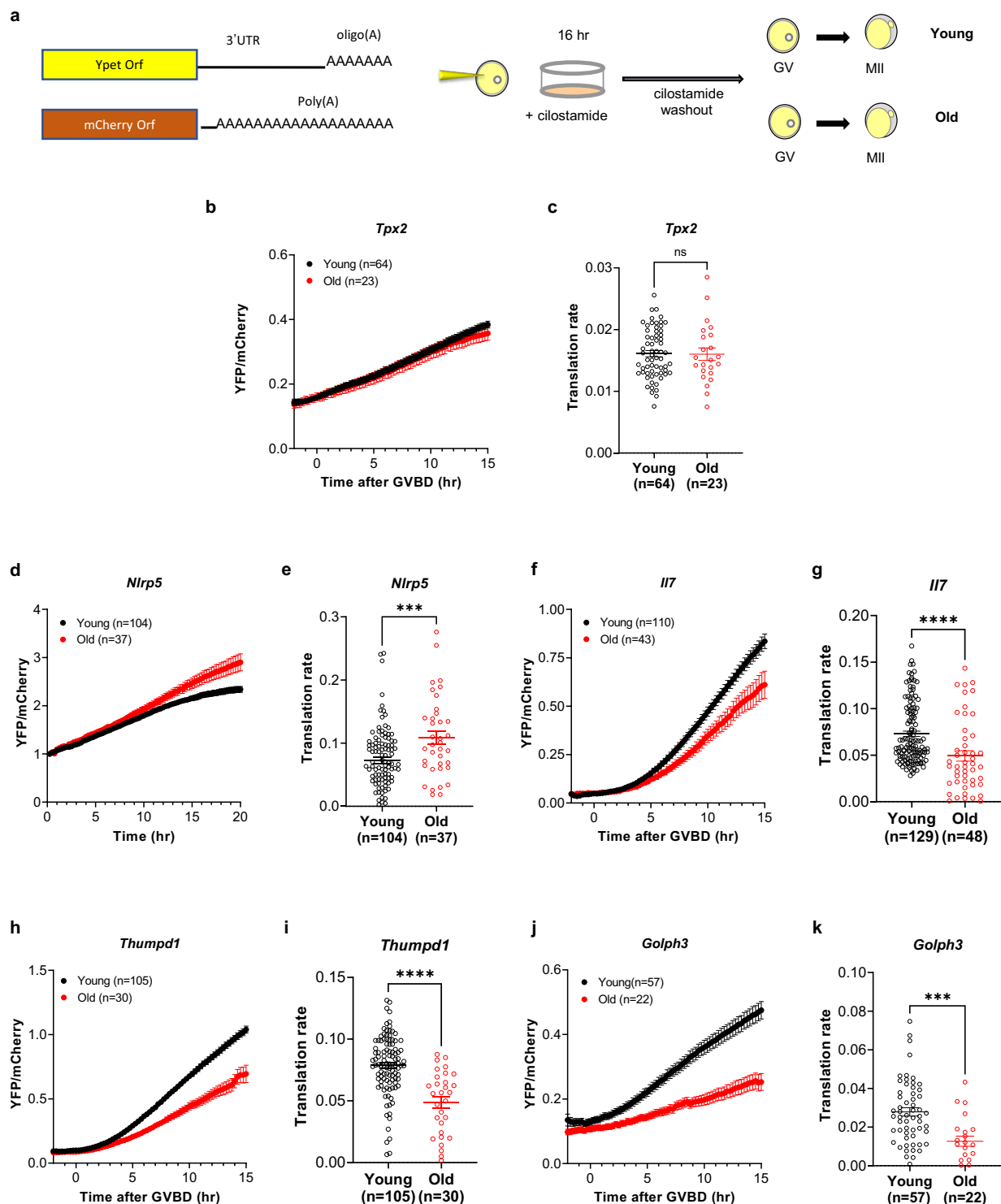


Fig. 2 | Complex alterations in translation are detected in old oocytes compared to young oocytes. a Scheme of YFP reporter assay. GV oocytes from young and old mice were injected with 12.5 ng/μl polyadenylated mCherry and 12.5 ng/μl of oligoadenylated YFP reporters, including *Tpx2*, *Nlrp5*, *Il7*, *Thumpd1*, and *Golph3* 3'-UTR. After overnight pre-incubation, oocytes were released in cilostamide-free medium, and YFP and mCherry signals were recorded by time-lapse microscopy every 15 min for 20 h during maturation. The YFP signals were normalized by the level of mCherry signals. **b, d, f, h, j** The ratio of YFP/mCherry signal for each oocyte was plotted according to the incubation time (**d**) or with time of GVBD set as 0 time

(**b, f, h, j**). **c, e, g, i, k** Translation rates were calculated for each oocyte by linear regression of the reporter data between 5 and 10 h (**b, j**), between 7 and 12 h after GVBD (**f, h**), or between 15 and 20 h after incubation time (**d**). Experiments were repeated three times with different batches of oocytes from different cohorts of aging mice and the data are shown as the mean ± SEM. Two-tailed unpaired Student's *t* tests were used to evaluate statistical significance, ns not significant, **e** ****P* = 0.0008, **g** *****P* < 0.0001, **h** *****P* < 0.0001, **k** ****P* = 0.0002. Source data are provided as a Source Data file.

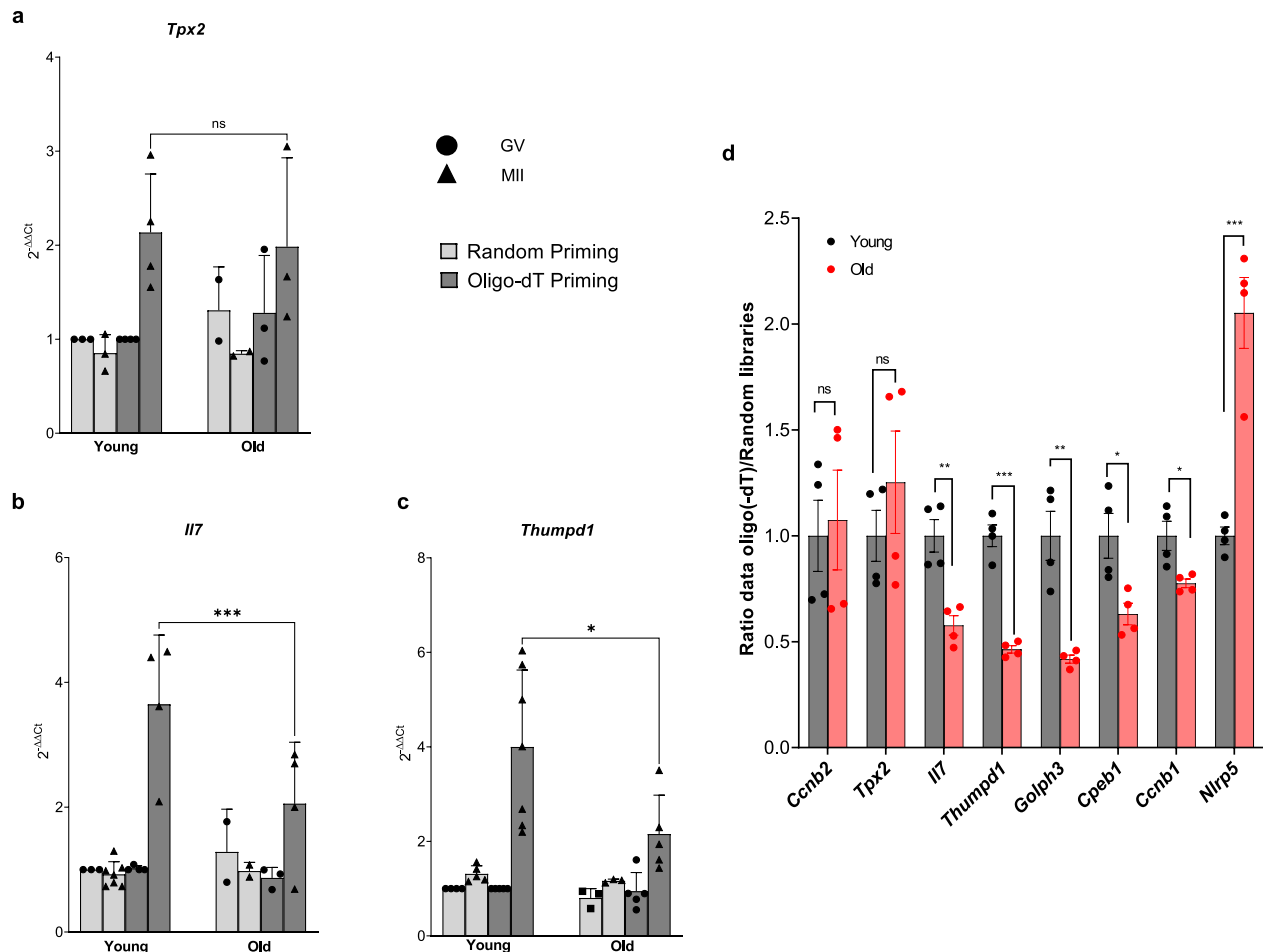


Fig. 3 | Endogenous mRNA Polyadenylations are altered with maternal aging.

a–c RNA of GV or MII oocytes from young or old mice was reverse-transcribed using random hexamer or oligo(-dT) primers, and quantitative PCR was performed with gene-specific primers. Data are normalized by the average expression of *Dppa3*, *Rpl19*, *Actb*, and *Eif4a1* as detailed in “Methods”. **a** $n = 3$ (GV young random), 3 (MII young random), 4 (GV young oligo(-dT)), 4 (MII young oligo(-dT)), 2 (GV old random), 2 (MII old random), 3 (GV old oligo(-dT)), 3 (MII old oligo(-dT)) biologically independent samples are used. **b** $n = 3$ (GV young random), 7 (MII young random), 4 (GV young oligo(-dT)), 4 (MII young oligo(-dT)), 2 (GV old random), 2 (MII old random), 3 (GV old oligo(-dT)), 4 (MII old oligo(-dT)) biologically independent samples are used. **c** $n = 4$ (GV young random), 5 (MII young random), 5 (GV young oligo(-dT)), and 7 (MII young oligo(-dT)), 3 (GV old random), 3 (MII old random), 5 (GV old oligo(-dT)), 5 (MII old oligo(-dT)) biologically independent

samples are used. The data are shown as the mean \pm SD. Two-tailed paired Student’s *t* tests were used to evaluate statistical significance, ns not significant, $*P = 0.029$, $***P = 0.0003$. **d** The ratio of data from oligo(-dT)²⁴ and random primed RNA-Seq libraries between young and old oocytes is reported. Four biologically independent oligo(-dT) samples and two biologically independent random primed samples are used. The data are shown as the mean \pm SD. A significantly decreased ratio is detected for *Il7*, *Thumpd1*, *Ccnb1*, *Golph3*, and *Cpeb1* mRNAs. Conversely, putative changes polyadenylation of *Ccnb2* and *Tpx2* mRNAs is not affected. Two-tailed multiple unpaired *t* tests were used to evaluate statistical significance, ns not significant, $**P = 0.0032$ for *Il7*, $***P = 0.000061$ for *Thumpd1*, $**P = 0.0025$ for *Golph3*, $*P = 0.019$ for *Cpeb1*, $*P = 0.020$ for *Ccnb1*, $***P = 0.00087$ for *Nlrp5*. Source data are provided as a Source Data file.

movement as the cumulus expands. Therefore, we used Renilla luciferase (RL) reporters fused with the 3'-UTR of target mRNA injected together with firefly luciferase (FL) into oocytes while still surrounded by cumulus cells (COCs) (Supplementary Fig. 7a). At the end of the incubation, oocytes were denuded, lysed, and used for luciferase assay. In all cases, the translation of reporters was increased from GV to MII (Supplementary Fig. 7b–d). In agreement with the denuded oocyte data, translation of *Il7* and *Thumpd1* was again significantly decreased in old MII oocytes compared with young MII oocytes (Supplementary Fig. 7c, d), whereas no difference in *Tpx2* translation was detected (Supplementary Fig. 7b). Thus, maintaining somatic/germ cell interaction does not rescue the defective translation.

Endogenous polyadenylation of mRNAs is decreased in old oocytes

In oocytes, activation of translation is dependent on the elongation of the poly(A) tail of an mRNA. To assess this property, we compared the

polyadenylation state of the endogenous *Tpx2*, *Il7*, and *Thumpd1* mRNAs in young and old oocytes using a strategy where qPCR signals from cDNA synthesized by either oligo(-dT) or random priming are compared. This is a widely employed assay when there are a limited number of cells available⁴³. As reported in Fig. 3a–c, the three transcripts show an apparent increase in MII versus GV with oligo(-dT) priming, whereas no significant changes were observed with random priming. This is consistent with the hypothesis that the polyadenylation of the three transcripts increases during oocyte maturation. More importantly, when comparing young and old oocytes, the signals from oligo(-dT) priming were significantly decreased for both *Il7* and *Thumpd1* mRNAs (Fig. 3b, c), whereas *Tpx2* polyadenylation was again unchanged (Fig. 3a). These data indicate that endogenous polyadenylation is defective in old oocytes, a finding consistent with the decreased translation detected with the reporter assays. To extend the correlation oligo(-dT)/random priming to additional mRNAs, we compared the deposited MII data obtained with oligo(-dT) priming

and our random priming dataset. The ratio of oligo-(dT)/random priming is comparable in young and old MII samples for most of the genes. However, significant differences in the ratio were detected for a subgroup of transcripts. These include the transcripts coding for *Il7*, *Thumpd1*, *Golph3*, and *Nlrp5*. Also, changes were detected for *Cpeb1* and *Ccnb1* (see below), while no differences in the ratio were observed for *Tpx2* and *Ccnb2* (Fig. 3d). Thus, these altered ratios are consistent with defective mRNA polyadenylation during aging.

Translation of CPEB1 is decreased in old oocytes

Polyadenylation of mRNAs and their translation during oocyte maturation, in large part, depends on the function of the RNA-binding protein (RBP) CPEB1²⁰. This RBP interacts with *cis*-acting elements located in the 3'-UTR of an mRNA and assembles a complex that promotes adenylation. Putative CPEs were identified in *Il7*, *Thumpd1*, and *Golph3* mRNAs, but not in *Nlrp5* mRNAs. Moreover, RNA-IP with CPEB1 antibodies conclusively confirms specific CPEB1-binding to endogenous *Il7*, *Thumpd1*, and *Golph3* mRNAs in the oocyte (Supplementary Fig. 8). Therefore, we hypothesized that a defective function of CPEB1 may be a cause of decreased polyadenylation and translation of these mRNAs in aging oocytes. Indeed, the RiboTag IP/RNA-Seq data indicate that, although not reaching statistical significance, the translation efficiency (TE)⁴⁴, defined as the ratio between ribosome-bound and total mRNA levels, for the *Cpeb1* mRNA is decreased ~50% in oocytes during maternal aging, whereas total mRNA levels are comparable between young and old oocytes (Fig. 4a). To confirm this observation, we performed RiboTag IP/qPCR using ovary extracts from young and old mice. Since the Cre recombinase in the RiboTag mouse is driven by the ZP3 promoter, the RiboTag IP of total ovary extract probes only translation in oocytes from secondary to antral follicles. Using this approach, total *Cpeb1* mRNA (input) did not differ between young and old ovaries (Fig. 4b); however, ribosome-bound mRNA was significantly decreased in ovaries from old mice (Fig. 4c) ($P < 0.01$). Decreased translation of the *Cpeb1* mRNA was further confirmed by a western blot of oocytes from young and old mice. CPEB1 protein levels are significantly decreased by ~50% in old oocytes compared to young (Fig. 4d, e). Of note, an “apparent” and significant decrease in CPEB1 levels is found in old oocytes with the aging transcriptome (Supplementary Fig. 1d) as well as an apparent decrease in polyadenylation (Fig. 3d). These results suggest that the decrease in CPEB1 protein expression in old oocytes is due to decreased translation throughout the growing follicle stages as well as during maturation.

An accelerated meiosis reentry in old oocytes is driven by increased Ccnb1 translation

CPEB1 is a critical RBP with complex functions during oocyte development. It is also considered a major regulator of progression through the meiotic cell cycle, given its role in the regulation of translation of critical cell cycle regulators, including cyclins. If aging were associated with a dysfunction in CPEB1, then an altered translation pattern of the prototypic CPEB1 target *Ccnb1* would be expected. This possibility was verified by injection of a reporter driven by the 3'-UTR of *Ccnb1* in oocytes from young and old mice and probing its rate of translation during GV stage. In fully grown GV oocytes, CPEB1 functions as a repressor of translation. Indeed, we found that the rate of translation of the *Ccnb1* reporter is increased in GV oocytes from old mice as compared to those from young mice (Fig. 5a, b). As a negative control, we used the translation of another cyclin, *Ccnb2*, which we have shown not to be repressed by CPEB1 in GV oocytes^{15,45}. No differences in the *Ccnb2* reporter signal were observed between young and old GV oocytes (Fig. 5c, d). Given the fact that CCNBI functions as a regulatory subunit of CDK1, the master regulator of meiosis progression, we tested whether a dysfunction in CPEB1 associated with aging would have any effects on the timing of meiotic cell cycle progression. We incubated oocytes in a maturation medium and recorded the time of GVBD using

time-lapse microscopy every 15 min. Under these conditions, reentry into meiosis is significantly accelerated by ~15 min in old oocytes (Fig. 6a). To verify a premature activation of CDK1, oocyte extracts were incubated with a CDK1 substrate protein phosphatase 1 (GST-PP1) peptide, and phosphorylation was measured by phospho-specific antibodies (pT320-PP1)^{46–48}. Considering that the maximum difference in GVBD time between young and old oocytes is 60 min after incubation (Fig. 6a) and CDK1 activation occurs before GVBD, we examined CDK1 activity in young and old oocytes after 45 min of removal of the PDE inhibitor. CDK1 activity was significantly increased in old compared with young oocytes (Fig. 6c, d). These results indicate that a loss in translational repression by CPEB1 during Prophase I causes an increased accumulation of CCNBI, therefore affecting the threshold levels of CDK1 activity as well as the timing of meiotic reentry.

Haploinsufficiency of CPEB1 in young mice recapitulates the translation and meiotic reentry phenotype of old oocytes

To test if haploinsufficiency of CPEB1 recapitulates the phenotypes associated with oocyte aging, we used conditional CPEB1 heterozygous (*Cpeb1*^{fl/+}; *Zp3-Cre*) mice. Western blotting detected a 50% decrease in CPEB1 protein in young CPEB1^{+/-} oocytes in GV state (Fig. 5e, f). This decrease in CPEB1 expression is comparable to that observed in old mice (Fig. 4d, e). To examine whether this partial loss of CPEB1 in young oocytes recapitulates the phenotypes associated with aging, we examined translation rate of *Ccnb1*, GVBD time, and CDK1 activity in this quiescent state. These measurements in CPEB1^{+/-} oocytes show that the rate of translation of the *Ccnb1* reporter is increased in GV oocytes (Fig. 5g, h), whereas no differences were observed with the *Ccnb2* reporter (Fig. 5i, j). Accelerated GVBD time and increased CDK1 activity were also observed in CPEB1^{+/-} oocytes (Fig. 6b, e, f). Although differences are not major, a clear gene dosage-dependent effect was observed when comparing heterozygous and homozygous null for the *Cpeb1* locus (Supplementary Fig. 9a). Thus, genetic manipulation of CPEB1 levels in young oocytes completely recapitulates all the phenotypes that we have described in old oocytes.

CPEB1 decreased function in old oocytes is rescued by injection of Cpeb1 mRNA

If de-repression of *Ccnb1* translation in GV oocytes were due exclusively to the decreased *Cpeb1* levels detected in old oocytes, increasing the accumulation of CPEB1 protein should rescue this translation phenotype. To test this possibility, GV oocytes were injected with in vitro-translated *Cpeb1* mRNA together with the *Ccnb1* reporter, and the accumulation of YFP was measured. Control experiments where CPEB1 protein levels were measured by western blot indicated an increase in CPEB1 protein levels up to twofold compared to control (Fig. 7a, b). Under these conditions, the increase in accumulation of the *Ccnb1* reporter in old oocytes was reversed by co-injection with the *Cpeb1* mRNA. The rate of translation in these co-injected oocytes was identical to young controls and significantly decreased when compared to old controls (Fig. 7c). Similar rescue of the de-repression was observed when young CPEB1 heterozygous oocytes were injected with reporter and *Cpeb1* mRNA (Fig. 7d).

The effect of decreased CPEB1 level on translation during oocyte maturation and fertility

Upon reentry into meiosis, CPEB1 switches its function from repressor to activator of translation. We tested whether translation of *Ccnb1* during maturation is also affected with maternal aging, as we have shown for *Il7*, *Thumpd1*, and *Golph3* (Fig. 2f–k). The rate of translation of the *Ccnb1* reporter was significantly decreased in old oocytes during maturation (Fig. 8a, e), whereas no differences in *Ccnb2* were observed (Fig. 8b, f). Decreased translation of *Ccnb1* reporter was also detected in young oocytes carrying a CPEB1 haploinsufficiency, with no significant change in *Ccnb2* reporter translation during

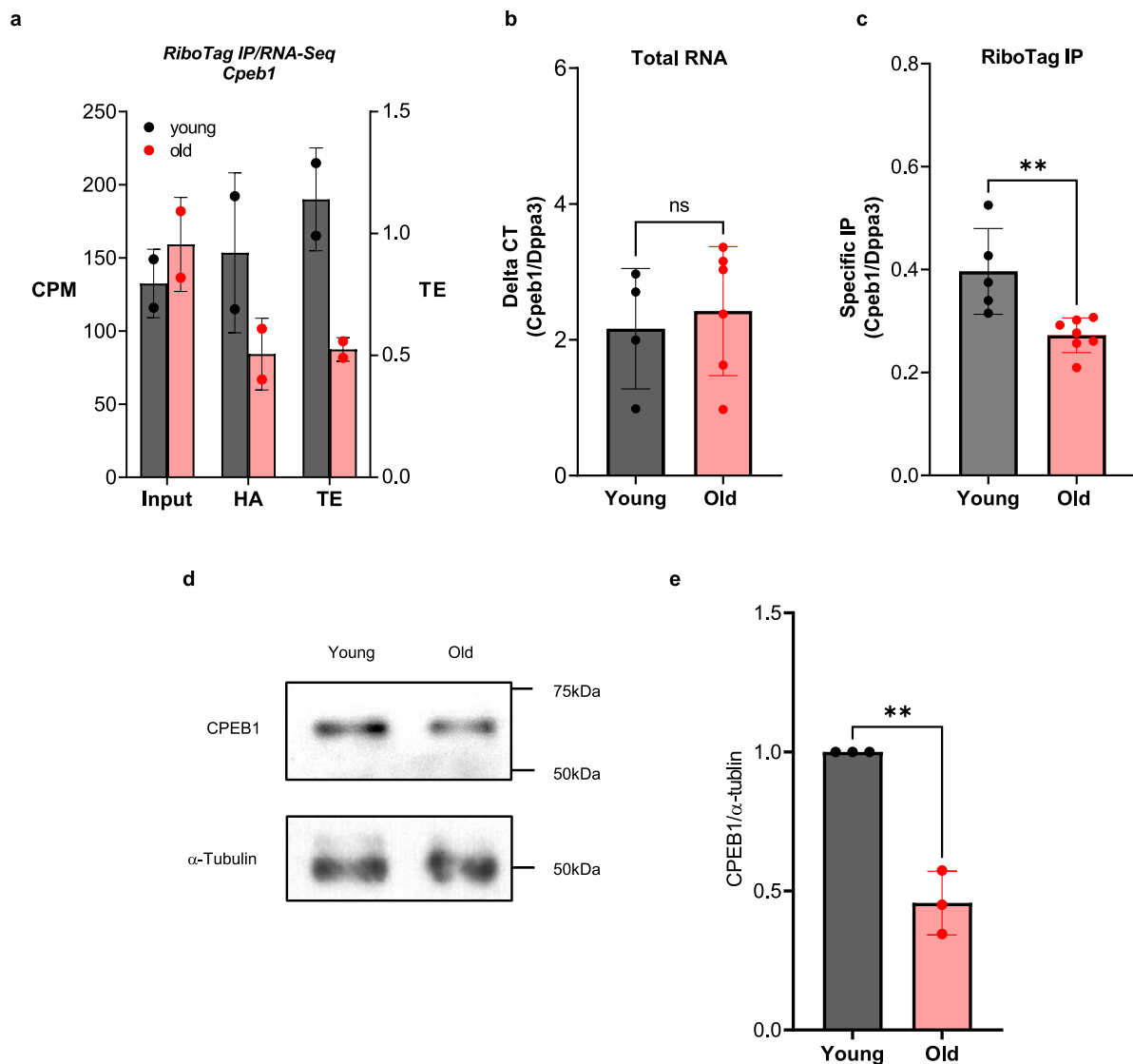


Fig. 4 | Translation of CPEB1 mRNA and protein is decreased in old oocytes.

a MII oocytes were collected from young and old *RiboTag^{FF};Zp3-Cre* mice and RiboTag IP followed by RNA-Seq was performed as described in “Methods”. The average CPM for total transcripts (Input) and ribosome loading of transcripts (HA) are reported. TE was calculated as the ratio between ribosome-associated and total mRNA CPM. Two independent biological samples were used in this analysis. **b, c** Ovaries were collected from young and old *RiboTag^{FF};Zp3-Cre* mice and RiboTag IP followed by RT-qPCR was performed as described in “Methods”. *Dppa3* was used as a reference gene. Input data (**b**) and ribosome-loading mRNA (**c**) are reported. **b** $n = 4$ (young), 6 (old) biologically independent samples are used. **c** $n = 5$ (young), 7 (old) biologically independent samples are used. RT-qPCR reactions

were run in triplicate. The bars represent the mean \pm SD. Two-tailed unpaired Student’s *t* tests were used to evaluate statistical significance, ns not significant, $**P = 0.0048$. **d, e** CPEB1 protein expression in GV oocytes from young and old mice. Accumulation of α -tubulin was used as a control. Oocytes were lysed in sample buffer and used for western blot analysis. Twenty-five oocytes per lane were loaded for the experiment. A representative of three experiments is reported. A graph shows quantification of a western blot on three independent biological replicates. The data are reported as the mean \pm SD. CPEB1/ α -tubulin ratios were expressed as fold changes over young controls. Two-tailed unpaired Student’s *t* tests were used to evaluate statistical significance, $**P = 0.0012$. Source data are provided as a Source Data file.

oocyte maturation (Fig. 8c, d, g, h). In both old oocytes and oocytes with haploinsufficiency, overexpression of *Cpeb1* rescued the decreased *Ccnb1* reporter translation (Fig. 7e, f). Again, there was a *Cpeb1*-gene dosage effect of CPEB1 on the translation of *Ccnb1* reporter (Supplementary Fig. 9b). Translation of *Il7*, *Thumpd1*, and *Golph3* reporters was also significantly decreased in CPEB1^{+/-} oocytes during maturation (Fig. 9b–d, f–h) while the translation of *Tpx2* was unchanged (Fig. 9a, e). All these results are fully consistent with the result of RNA-IP with CPEB1 antibodies (Supplementary Fig. 8). Thus, dysfunction of CPEB1 during maternal aging affects translation during maturation as well.

We have previously shown that decreased *Ccnb1* translation causes increased aneuploidy rate and infertility⁴⁶. Given that change in

timing of meiosis reentry and decreased translation of *Ccnb1* in oocytes causes infertility, we tested whether a partial loss in CPEB1 expression in oocytes may affect fertility by mating CPEB1^{+/-} female mice with wild-type male mice. Conditional CPEB1 knockout after birth in female mice leads to complete infertility^{15,49}. Although there was no difference in the number of oocytes retrieved (Fig. 10a), maturation rate, and diameter of oocytes between CPEB1^{+/+} and CPEB1^{+/-} mice (Supplementary Fig. 10a–c), fertility was significantly decreased 3 months after mating (Fig. 10b) and CPEB1^{+/-} mice progressively produced significantly fewer pups compared with CPEB1^{+/+} mice (Fig. 10c). CPEB1^{+/-} mice also show a decrease in the number of pregnancies (Fig. 10d). The age of first pregnancy of CPEB1^{+/+} and CPEB1^{+/-} mice and the body weight of pups were comparable (Supplementary

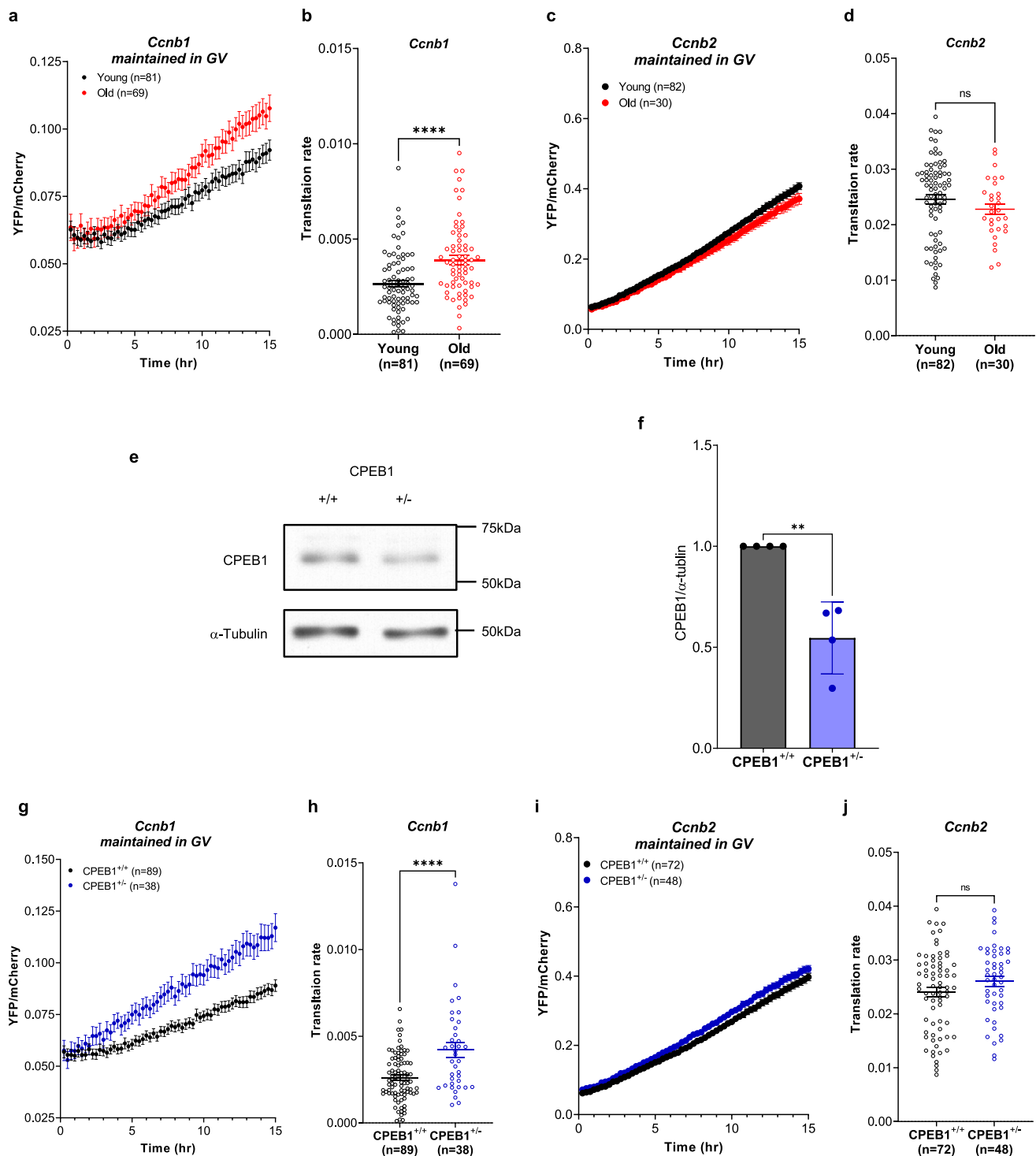


Fig. 5 | Decreased CPEB1 expression de-represses *Ccnb1* translation during the GV stage. **a–d**, **g–j** GV oocytes from young and old mice (**a–d**) or *Cpeb1*^{+/+}*Zp3Cre* mice (CPEB1^{+/+} oocytes) and *Cpeb1*^{+/-}*Zp3Cre* mice (CPEB1^{+/-} oocytes) (**g–j**) were injected with polyadenylated mCherry and YFP-*Ccnb1* 3'-UTR (**a, b, g, h**) or YFP-*Ccnb2* 3'-UTR (**c, d, i, j**). After 3 h of pre-incubation, oocytes were maintained in GV stage with cilostamide treatment. YFP and mCherry signals were recorded by time-lapse microscopy every 15 min for 15 h. The YFP signals were normalized by the level of mCherry signals. **a, c, g, i** YFP/mCherry signal in each oocyte was plotted depending on the incubation time. **b, d, h, j** Translation rate was calculated for each oocyte by linear regression of the reporter data between 3 and 13 h. Experiments

were repeated three times and the data are shown as the mean \pm SEM. Two-tailed unpaired Student's *t* tests were used to evaluate statistical significance, ns not significant, *****P* < 0.0001. **e, f** CPEB1 protein expression in CPEB1^{+/+} GV oocytes and CPEB1^{+/-} GV oocytes. Accumulation of α -tubulin was used as a control. Oocytes were lysed in sample buffer and used for western blot analysis with 30 oocytes per lane loaded for the experiment. **e** A representative of four experiments is reported. **f** A graph shows the quantification of four independent western blot analyses. The bar represents mean \pm SD. CPEB1/ α -tubulin ratios were expressed as fold changes over CPEB1^{+/+} oocytes. Two-tailed unpaired Student's *t* tests were used to evaluate statistical significance, ***P* = 0.0023. Source data are provided as a Source Data file.

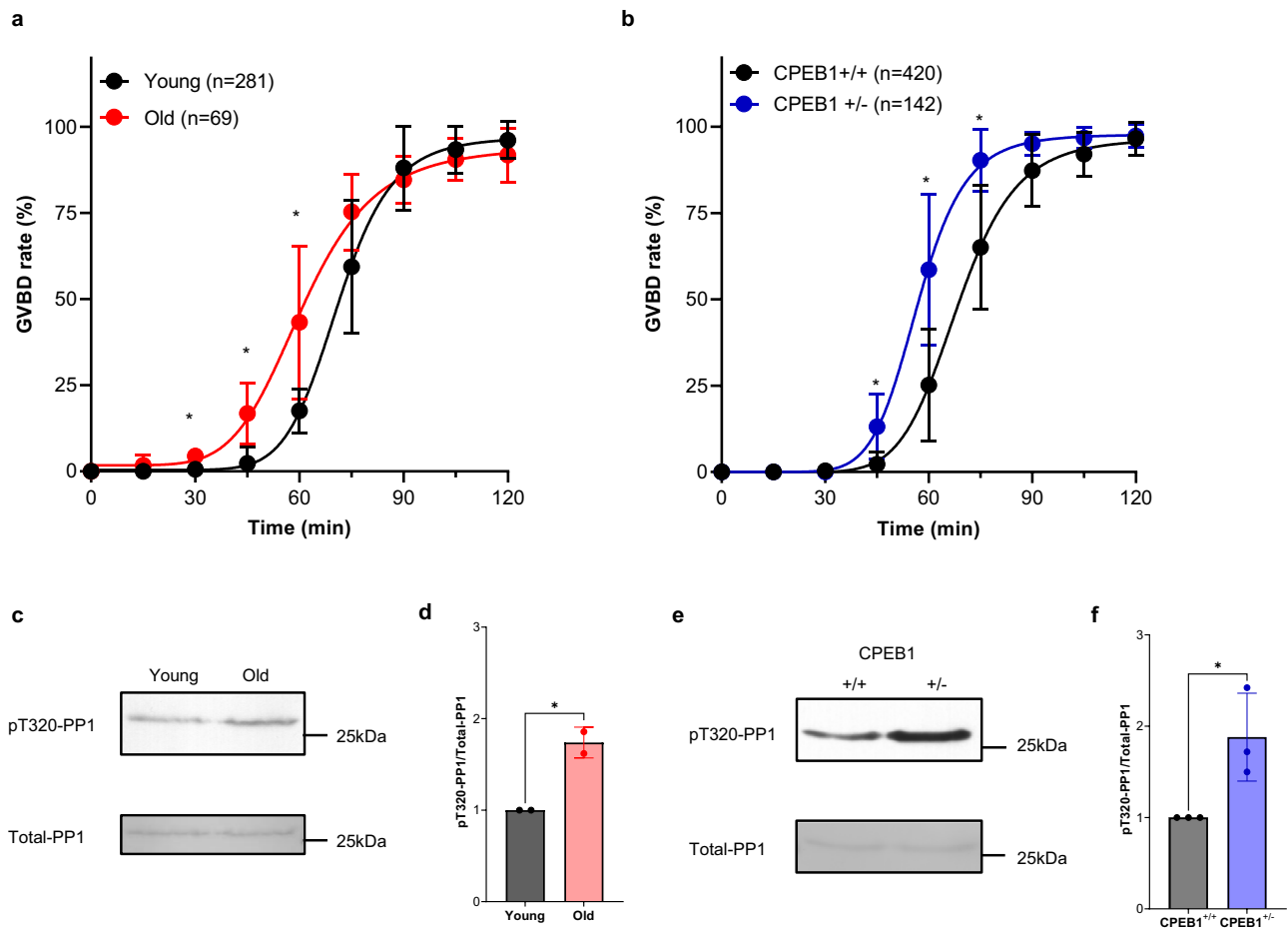


Fig. 6 | Decreased CPEB1 expression accelerates meiosis reentry. **a, b** GV oocytes from young and old mice (**a**), or GV oocytes from *Cpeb1*^{+/+}; *Zp3Cre* mice (CPEB1^{+/+} oocytes) and *Cpeb1*^{+/-}; *Zp3Cre* mice (CPEB1^{+/-} oocytes) (**b**) were incubated with cilostamide-free medium and brightfield images were captured every 15 min. The cumulative GVBD times were plotted. Experiments were repeated at least three times, and the data are shown as the mean \pm SD. Two-tailed multiple unpaired Student's *t* tests were used to evaluate statistical significance at each time point. **a** $P=0.00032$ for 30 min, $P=0.0076$ for 45 min, $P=0.016$ for 60 min. **b** $P=0.0036$ for 45 min, $P=0.0051$ for 60 min, $P=0.019$ for 75 min. **c–f** CDK1 activity were measured using Kinase assays. Young and old GV oocytes (**c, d**), or CPEB1^{+/+} and CPEB1^{+/-} GV oocytes (**e, f**) were incubated with cilostamide-free medium for 45 min.

After oocytes were lysed by freezing and thawing, oocytes were incubated with GST-PP1 fragment as a substrate for 30 min. Oocytes were lysed in a sample buffer and used for western blot analysis. T320 PP1 phosphorylation was detected by a phospho-specific antibody (pT320-PP1). The level of total substrate loaded was evaluated by Ponceau S staining (Total PP1). Ten oocytes per lane were loaded for the experiment. **c, e** A representative of experiments is reported. **d, f** A graph shows the quantification of two or three independent western blot analyses. The data are shown as the mean \pm SD. pT320-PP1/total PP1 ratios were expressed as fold changes over young controls. Two-tailed unpaired Student's *t* tests were used to evaluate statistical significance, **d** $*P=0.025$, **f** $*P=0.033$. Source data are provided as a Source Data file.

Fig. 10d, e). Thus, *Cpeb1* haploinsufficiency in young mice causes a decrease in oocyte quality and recapitulates some of the phenotypes associated with CPEB1 dysfunction in maternal aging.

Discussion

Using different complementary approaches, we have determined that maternal aging is associated with a disruption of the mRNA translation program executed during oocyte maturation. Approximately 5% of the mRNAs present in the oocyte are incorrectly translated during maturation. Although changes in translation are not profound, we propose that the cumulative effects of inefficient translation and consequently altered proteostasis have an impact on oocyte quality. Mechanistically, we document that translation of the mRNA coding for an RBP critical for translation regulation in the oocyte, CPEB1, is affected, resulting in decreased accumulation of this protein. This, in turn, results in altered translation in oocytes and aberrant progression through the meiotic cell cycle. The association of CPEB1 with these phenotypes detected in old oocytes is recapitulated by a model of haploinsufficiency of CPEB1 where similar reductions in

CPEB1 protein are induced in young oocytes. Moreover, increasing CPEB1 levels in old oocytes rescues these translation phenotypes. Therefore, we believe that altered CPEB1 function, likely arising during oocyte growth, is the molecular defect underlying some of the phenotypes associated with decreased oocyte fitness during maternal aging. Together with decreased production of oocytes due to follicle depletion, the altered CPEB1-dependent disruption of de novo protein synthesis may recapitulate the decreased fertility observed with aging.

Our RiboTag IP/RNA-Seq data show an alteration in ribosome loading in old oocytes when compared to young oocytes. Although the power of this analysis was limited by the availability of old oocytes for molecular analysis, our data are internally consistent. For instance, the TE in control young oocytes of this study is highly correlated to that measured in other datasets we have generated^{14,15}, as well as the RNA-Seq data on translation reported by others⁵⁰. Comparison between our data and the translome of Pan et al²⁴ shows consistent effects on some genes. Moreover, GO analysis predicts a highly significant disruption in the translation of components necessary for mitochondrion biogenesis/function. Defective

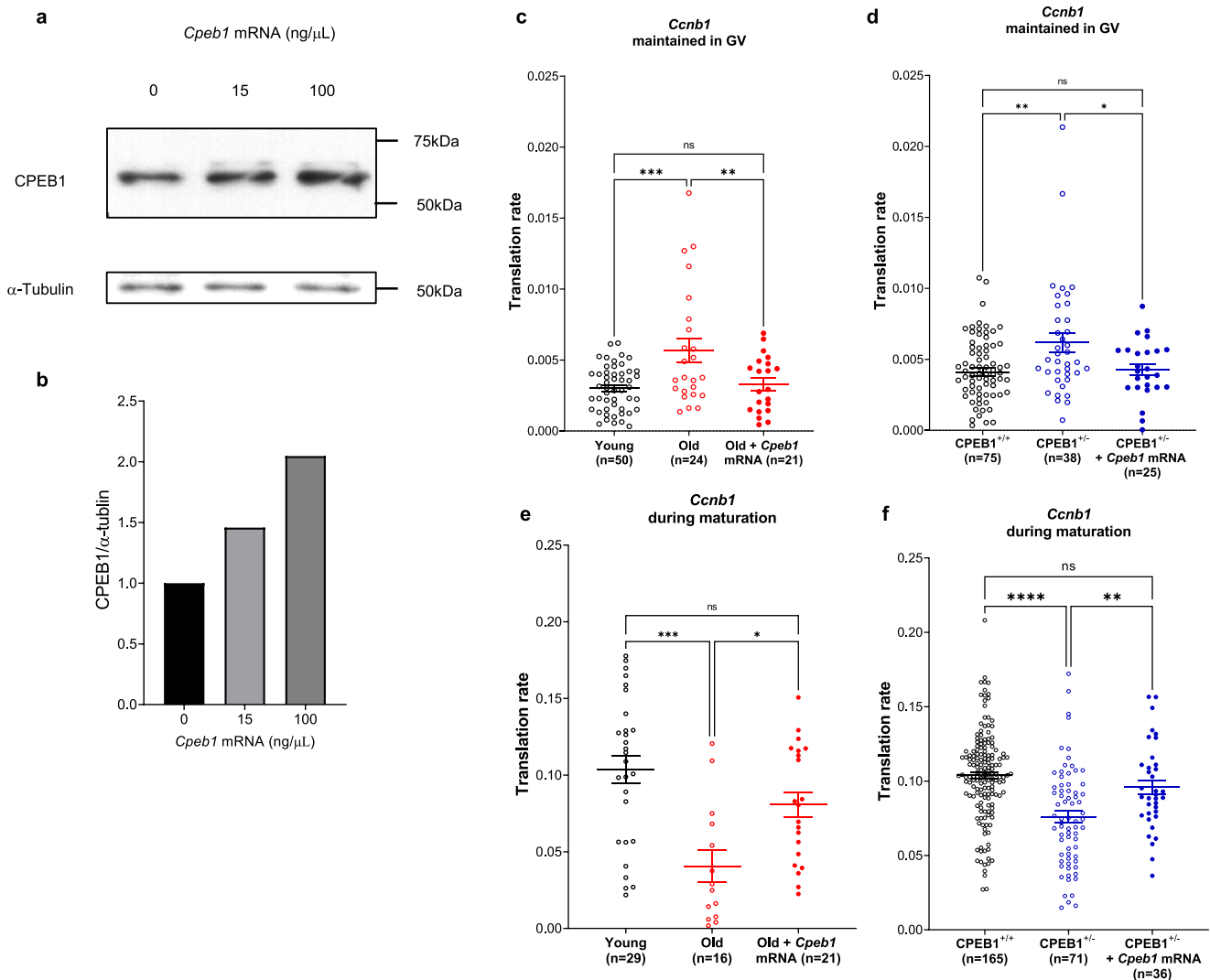


Fig. 7 | CPEB1 decreased function in old oocytes can be rescued by injection of *Cpeb1* mRNA. **a, b** CPEB1 protein expression in GV oocytes injected with *Cpeb1* mRNA at different concentrations. Accumulation of the endogenous α-tubulin was used as a control. Oocytes were lysed in a sample buffer and used for western blot analysis. In total, 30 oocytes per lane were loaded for the experiment. **b** A graph shows quantification of a single western blot analysis. CPEB1/α-tubulin ratios were expressed as fold changes over control. **c–f** GV oocytes from young and old mice, or *Cpeb1*^{+/+}; *Zp3Cre* mice (CPEB1^{+/+} oocytes) and *Cpeb1*^{+/-}; *Zp3Cre* mice (CPEB1^{+/-} oocytes) were injected with polyadenylated mCherry, *YFP-Ccnb1* 3'-UTR, and *Cpeb1* mRNA (100 ng/μl). After overnight pre-incubation, oocytes were maintained in GV

stage with cilostamide treatment (**c, d**), or released in the cilostamide-free medium for maturation (**e, f**). YFP and mCherry signals were recorded by time-lapse microscopy every 15 min for 20 h. The YFP signals were normalized by the level of mCherry signals. The translation rate was calculated for each oocyte by linear regression of the reporter data. Experiments were repeated three times and the data are shown as the mean ± SEM. One-way ANOVA were used to evaluate statistical significance, ns not significant, **c** ***P* = 0.0076, ****P* = 0.0002, **d** **P* = 0.034, ***P* = 0.0015, **e** **P* = 0.025, ****P* = 0.0001, **f** ***P* = 0.0048, *****P* < 0.0001. Source data are provided as a Source Data file.

mitochondrion function is a hallmark of aging³⁷, and altered translation of mitochondrial proteins have been reported. The prediction of an altered ribosome-associated protein acetylation and ribosome biogenesis also is supported by our finding of altered polyadenylation of *Thumpd1* mRNA and altered translation of a reporter driven by the 3'-UTR of *Thumpd1*. However, comparison of our data with those recently reported by others²⁷, unfortunately shows little or no overlap, with the possible exception of a decrease in *Sgk1* translation. Although that report documented altered translation of 38 mRNAs (FDR < 0.1; 8 mRNAs with FDR < 0.05), we detect more widespread defects that amount to 726 mRNAs if the same cutoff is applied (FDR < 0.1, 256 mRNAs with FDR < 0.05). The reason for this discrepancy is at presently not clear. It should be noted that Del Llano et al.²⁷ assessed translation immediately after in vitro GVBD, a time during which activation/repression of translation is minimally different from that in quiescent oocytes¹⁵. Conversely, we assessed

changes in translation in MII oocytes matured in vivo, when differences in translation have reached a maximum.

Collectively, our data point to a defective function of CPEB1 as one of the molecular causes of altered translation. This conclusion is based on (1) Altered translation of the *Cpeb1* mRNA in oocytes and related 50% decrease in CPEB1 protein; (2) Defective translation of *Ccnb1*, *Il7*, *Thumpd1*, and *Golph3* mRNAs, which are all bona fide CPEB1 targets; (3) Altered polyadenylation of *Ccnb1*, *Il7*, *Thumpd1*, and *Golph3*; (4) Altered parameters of oocyte reentry into the cell cycle predicted by altered regulation of CCNB1 synthesis; (5) A defective accumulation of CPEB1 in young oocytes completely recapitulates the translation and meiotic progression observed in old oocytes, and increasing CPEB1 protein levels in old oocytes rescues the translation phenotypes. Therefore, our conclusions are based on multiple independent observations all converging on CPEB1 dysfunction during aging. It should be noted that, although not detected by some⁵¹, others have reported that

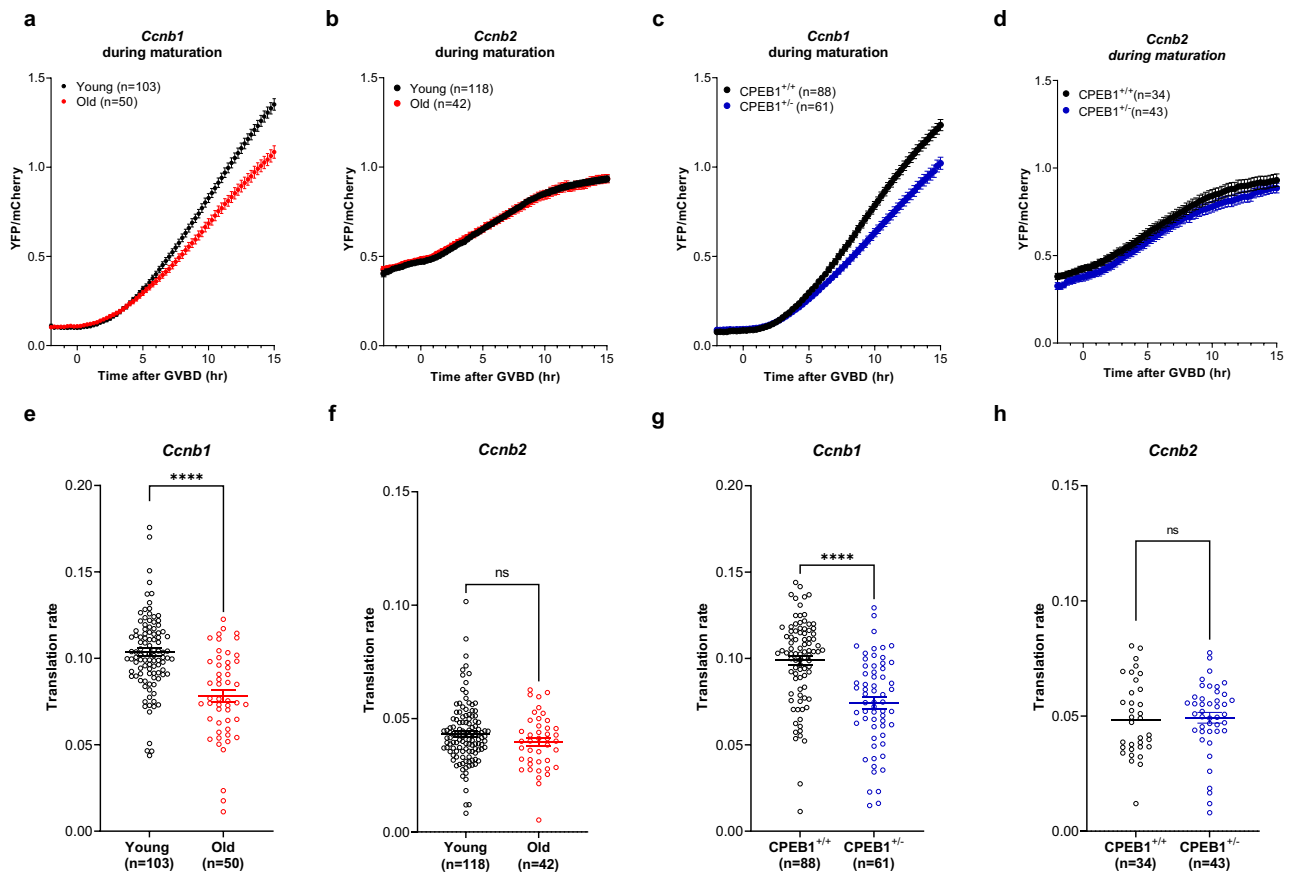


Fig. 8 | The effect of decreased CPEB1 level on *Ccnb1* translation during oocyte maturation. GV oocytes from young and old mice (a, b, e, f), or GV oocytes from *Cpeb1*^{+/+}*Zp3Cre* mice (*CPEB1*^{+/+} oocytes) and *Cpeb1*^{+/-}*Zp3Cre* (*CPEB1*^{+/-} oocytes) (c, d, g, h) were injected with 12.5 ng/μl polyadenylated mCherry and 12.5 ng/μl YFP-*Ccnb1* 3'-UTR (a, c, e, g) or YFP-*Ccnb2* 3'-UTR (b, d, f, h). After pre-incubation overnight, oocytes were released in the cilostamide-free medium for maturation. YFP and mCherry signals were recorded by time-lapse microscopy every 15 min for

20 h. The YFP signals were normalized by the level of mCherry signals. a–d YFP/mCherry signal in each oocyte was plotted depending on the time of GVBD. e–h Translation rate was calculated for each oocyte by linear regression of the reporter data between 5 and 10 h (a, c) or between 3 and 7 h (b, d). Experiments were repeated three times and the data are shown as the mean ± SEM. Two-tailed unpaired Student's *t* tests were used to evaluate statistical significance, ns not significant, *****P* < 0.0001. Source data are provided as a Source Data file.

maternal aging causes an accelerated reentry into the meiotic cell cycle^{52,53}, as we have detailed here. Moreover, although the detected effects associated with *Cpeb1* haploinsufficiency are not major, we consistently observe a *Cpeb1*-gene dosage-dependent effect, reinforcing the validity of our observations.

Bioinformatic analysis of the properties of the transcripts affected during aging indicates that not all associated 3'-UTRs contain a putative CPE. Of the 126 3'-UTRs analyzed, we can identify a putative CPE in 84, whereas this cis-acting element is not detected in 42 3'-UTRs. This is documented by the analysis of *Nlrp5* mRNA. The translation of the endogenous *Nlrp5* mRNA is increased in our dataset, and an apparent transcript increase is detected in the deposited aging transcriptome. Moreover, reporter data show defective repression of *Nlrp5* translation. The *Nlrp5* 3'-UTR does not contain discernible CPE elements, and the endogenous *Nlrp5* is not immunoprecipitated in a RIP assay; thus, mechanisms other than CPEB1-mediated translation may be altered. That not all affected transcripts contain a CPE is also inferred with the analysis of the mRNAs coding for the mitochondrial ribosomal proteins. These findings suggest that either translation of some mRNA is indirectly affected by a dysfunctional CPEB1 or that more complex events disrupt the translation of maternal mRNAs during aging. In this latter scenario, a CPEB1-dependent component acts in parallel with an alteration of other regulatory circuits controlling translation. The RBPs involved, as well as the exact molecular mechanisms implicated, require further investigation.

Given the increased translation in GV oocytes followed by a decreased rate of translation during maturation, we calculate that the overall activation of *Ccnb1* mRNA translation is decreased by 50% in old oocytes. This decrease is substantial and likely disruptive of meiotic progression. For instance, we find that a 30% decrease in *Ccnb1* mRNA translation in *Ccnb2*-loss of function is associated with a significant increase in aneuploidy⁴⁶. The kinetochore-microtubule attachment is regulated by CDK1 activity and a change in CDK1 activity leads to lagging chromosomes at anaphase I⁵⁴. In addition, studies have reported that pharmacological acceleration of meiosis I cause higher rate of aneuploidy^{55,56}. Thus, change in timing of meiosis reentry and altered CDK1 activation may be linked to the aneuploidy described in aged oocytes.

The post-transcriptional regulation controlling *Cpeb1* mRNA translation has not been investigated extensively. However, CPEB1 binds to its own mRNA (Supplementary Fig. 8) and represses its own translation in GV oocytes⁵⁷. Moreover, an element that binds AU-rich binding factor 1 (AUF1) has been described, and a function for microRNA-dependent modulation of *Cpeb1* has been described in neuroblastoma cells⁵⁸. Thus, several possible mechanisms may be causing a decreased translation of *Cpeb1* during oocyte growth and maturation, mechanisms that require further investigation.

Collectively, our data strongly support the concept that a disruption in the translation program in mouse oocytes is associated with maternal aging. Moreover, we provide evidence that an altered

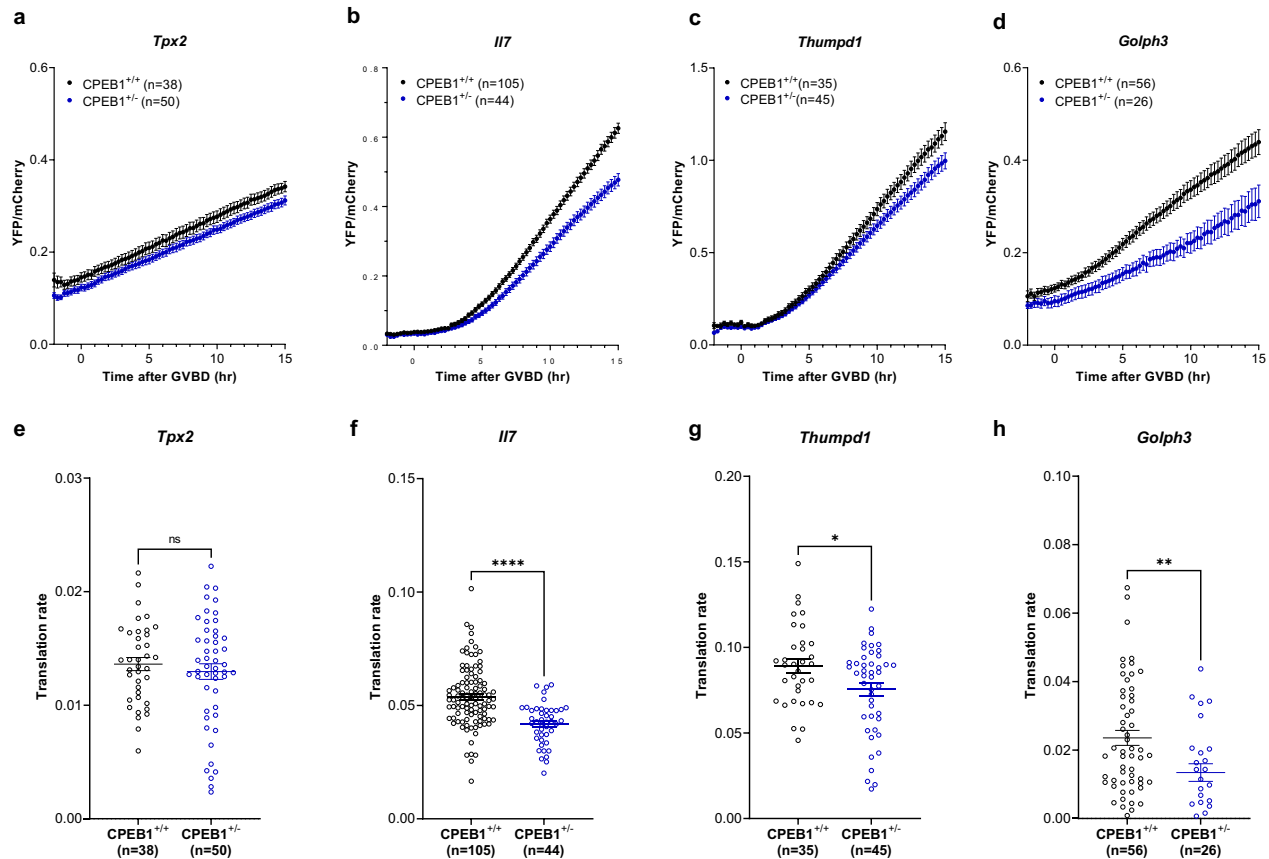


Fig. 9 | Haploinsufficiency of CPEB1 recapitulates the decreased translation during oocyte maturation. GV oocytes from *Cpeb1^{+/+};Zp3Cre* mice (CPEB1^{+/+} oocytes) and *Cpeb1^{+/-};Zp3Cre* mice (CPEB1^{+/-} oocytes) were injected with polyadenylated mCherry and *YFP-Tpx2* 3'-UTR (a, e), *YFP-Il7* 3'-UTR (b, f), *YFP-Thumpd1* 3'-UTR (c, g), or *YFP-Golph3* 3'-UTR (d, h). After pre-incubation overnight, oocytes were released in the cilostamide-free medium for maturation. YFP and mCherry signals were recorded by time-lapse microscopy every 15 min for 20 h. The YFP signals were normalized by the level of mCherry signals. a–d YFP/mCherry signal in

each oocyte was plotted depending on the time of GVBD. e–h Translation rate was calculated for each oocyte by linear regression of the reporter data between 5 and 10 h (a, d) or between 7 and 12 h after GVBD (b, c). Experiments were repeated three times and the data are shown as the mean \pm SEM. Two-tailed unpaired Student's *t* tests were used to evaluate statistical significance, ns not significant, **P* = 0.017, ***P* = 0.0070, *****P* < 0.0001. Source data are provided as a Source Data file.

stoichiometry of CPEB1 protein may be one of the molecular defects causing altered maternal mRNA translation in aging oocytes. In addition to being consistent with other observations, the fact that these phenotypes can be rescued by overexpression of CPEB1 and recapitulated by a model of *Cpeb1* haploinsufficiency in oocytes from young females provides compelling support of our overall hypothesis. It should be also noted that heterozygous deletions of the *Cpeb1* gene in humans have been associated with Premature ovarian insufficiency^{59–62}, a view that further supports the *Cpeb1*-dependent phenotypes during aging. A disrupted CPEB1-dependent mode of the translation may not be the only mechanism, as preliminary evidence also suggests disruption of a CPEB1-independent component of translation. Further studies are required to determine how all these defects in the translation program cumulatively converge to disrupt oocyte quality and fertility.

It should be pointed out that altered translation is just one of the components associated with reproductive aging. Although not profound, the decreased oocyte quality and fertility in young mice associated with *Cpeb1* haploinsufficiency on a background of normal number of ovulated oocytes, likely compounds with the large decrease in the number of follicles that mature and the number of ovulated oocytes during aging. Thus, we propose that the overall decrease in fertility observed during aging is the sum or the compound effects of the altered number of oocytes produced and their defective developmental competence due to altered maternal mRNA translation.

Methods

Experimental animals

All experimental procedures involving animal models used were approved by the Institutional Animal Care and Use Committee of the University of California at San Francisco (AN182026-03A). All animals used were of the C57BL/6 inbred strain. Mice were housed in 12 h light/12 h dark cycle at the temperature of 18–23 °C with 40–60% humidity environment. Young mice used were 1-month-old females, whereas 12–15 months old retired female breeders were considered old mice. C57BL/6-*Zp3Cre*Rpl22tm1.1Ppsam (*RiboTag^{+/+};Zp3-Cre*) mice were obtained from Jackson Laboratories and bred as described previously²⁹. CPEB1-targeted mice were a gift from ref. ⁶³ and C57BL/6-*Cpeb1^{+/+};Zp3-Cre* female mice were bred in our facility.

Oocyte collection

Female mice were injected with 5 I.U. pregnant mare serum gonadotropin (PMSG; MyBioSource) to induce follicle growth and sacrificed 44 h after injection. The ovaries were dissected, and COCs were collected in media containing HEPES-modified minimum essential medium Eagle (Sigma-Aldrich, M2645) supplemented with 0.23 mM sodium pyruvate (Gibco, 11360070), penicillin–streptomycin (Genesee Scientific Corporation (GenClone), 25-512), and 3 mg/ml BSA (Sigma-Aldrich, SIAL-A3311), 6 mM sodium bicarbonate (JT-Baker, 3506-1), and a PDE inhibitor (1 μ M cilostamide (Calbiochem, 231085) or 2 μ M milrinone (Enzo ALK-270-083)). Aspiration through a glass

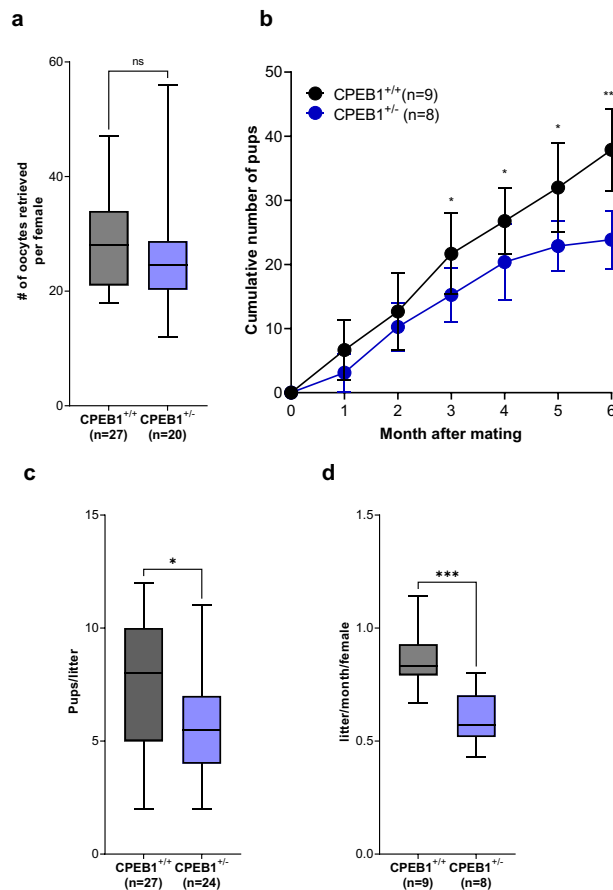


Fig. 10 | The effect of decreased CPEB1 level on mouse fertility. **a** *Cpeb1*^{+/+}; *Zp3Cre* mice (CPEB^{+/+} mice) and *Cpeb1*^{fl/fl}; *Zp3Cre* mice (CPEB^{+/-} mice) were primed with PMSG and ovaries were dissected 44 h later. GV oocytes from each pair of ovaries were counted. Data are reported as box and whisker plots. The central line denotes the median value, while the box refers to the 25th to 75th percentiles and whiskers mark minimum and max values. Unpaired Student's *t* tests were used to evaluate statistical significance, n.s. not significant. **b–d** CPEB^{+/+} and CPEB^{+/-} female mice were mated with WT male mice. Breeding was initiated when mice reached at least 8 weeks of age. **b** Cumulative number of pups per female derived from CPEB^{+/+} and CPEB^{+/-} mice was recorded. The data are reported as the mean ± SD. Two-tailed multiple unpaired Student's *t* tests were used to evaluate statistical significance at each time point. **P* = 0.027 for 3 months, **P* = 0.030 for 4 months, **P* = 0.0052 for

5 months, ****P* = 0.00011 for 6 months. **c** The number of pups per litter up to three pregnancies was recorded and data reported as box and whisker plots. The central line denotes the median value, while the box refers to the 25th to 75th percentiles and whiskers mark minimum and max values. The number of litters analyzed is included among brackets. Two-tailed unpaired Student's *t* tests were used to evaluate statistical significance, **P* = 0.030. **d** The frequency of parturition was measured and expressed as a number of litters per month per female. The data are plotted as box and whisker plots. The central line denotes the median value, while the box contains the 25th to 75th percentiles and whiskers mark minimum and max values. Two-tailed unpaired Student's *t* tests were used to evaluate statistical significance, ****P* = 0.0008. Source data are provided as a Source Data file.

pipette allowed for the removal of the surrounding cumulus cells. Denuded oocytes were maintained at the GV stage in α -MEM (Gibco, 12561-056) supplemented with 0.23 mM sodium pyruvate, penicillin–streptomycin, and 1 μ M cilostamide (or 2 μ M milrinone) at 37 °C under 5% CO₂. For the collection of in vivo MII oocytes, female mice were injected with 5 I.U. of PMSG followed by 10 I.U. human chorionic gonadotropin (hCG; Goldline Labs) 48 h after PMSG injection, and after 13 h, sacrificed for ovulated oocytes retrieval from the fallopian tubes.

RiboTag IP

Oocytes from *RiboTag*^{fl/fl}; *Zp3-Cre* female mice stimulated with 5 I.U. PMSG followed by 10 I.U. hCG, or ovaries from *RiboTag*^{fl/fl}; *Zp3-Cre* female mice stimulated with 5 I.U. PMSG only was used for RiboTag-immunoprecipitation. Oocytes were collected in 10 μ l of 1 \times PBS (Invitrogen, AM9625), supplemented with 0.1% w/v polyvinylpyrrolidone (PVP; Sigma, P0930), 0.1% v/v Cyclohexamide (CHX; Sigma C7698), and 250 U RNaseOUT (Invitrogen 10777-019), then flash-frozen in liquid nitrogen, and stored at –80 °C. Ovaries were collected whole, flash-frozen in liquid nitrogen, and

stored at –80 °C. To prepare samples for the IP, the appropriate volume (80 μ l per sample) of Dynabeads™ Protein G (Invitrogen, 10004D) was washed two times in 250 μ l homogenization buffer (HB: 50 mM Tris–HCl pH 7.4, 100 mM KCl, 12 mM MgCl₂ and 1% v/v NP-40) on a rotor at 4 °C for 5 min per wash. Two additional washes were performed with 250 μ l supplemented HB (sHB: HB supplemented with 1 mM DTT (sigma 646563), 1 \times HALT protease inhibitor (Fisher P178441), 200 units/ml RNaseOUT, 200 units/ml RNasin (Promega N2115), 100 μ g/ml CHX) on a rotor at 4 °C for 5 min per wash. Following the final wash, the beads were eluted back to the original volume with sHB. Oocyte samples were thawed and pooled to yield a total of 200 oocytes per replicate, and 300 μ l sHB was added to each pooled sample. To lyse the cells, samples were vortexed for 30 s and the homogenates were centrifuged for 15 min at 20,817 \times *g* at 4 °C. Ovaries were homogenized in 300 μ l sHB and centrifuged likewise. To pre-clear the samples, the supernatants were transferred to new tubes, 20 μ l of washed beads were added to each supernatant, and samples were incubated on a rotor at 4 °C for 30 min. A magnetic rack was used to remove the beads, and 30 μ l (10%) of each pre-cleared lysate was collected and added

to 250 μ l RLT buffer (Qiagen, 74034) supplemented with 1 mM DTT to serve as the input samples. The input samples were frozen and kept at -80°C until RNA extraction. In total, 4 μ l (4 μ g) anti-HA.11 epitope tag antibody (1/75, Invitrogen, 26183) was added to each of the extracts and all samples were incubated on a rotor at 4°C for 4 h. Thirty microliters of washed beads were added to the samples and incubated overnight on a rotor at 4°C . The beads (now bound by HA-tagged ribosomes and the associated mRNAs) were washed four times in 750 μ l urea wash buffer (uWB: 50 mM Tris-HCl pH 7.4, 150 mM KCl, 12 mM MgCl_2 , 1% v/v NP-40, 1 \times protease inhibitors, 1 mM DTT, 40 U RNaseOUT, 40 U RNasin, 100 μ g/ml cycloheximide, and 1 M urea) on a rotor at 4°C for 10 min per wash. The bead slurry was then transferred to fresh tubes, pelleted via magnetic rack, and the uWB removed. To strip the mRNA complex off the beads, 250 μ l RLT buffer supplemented with DTT was added to each sample and samples were vortexed for 30 s. Finally, beads were pelleted and removed before RNA extraction was performed using the Rneasy Plus Micro Kit (Qiagen, 74034). Samples were eluted in 14 μ l of RNase-free water and used downstream for RNA-Seq or RT-qPCR analysis.

RNA-Seq

RNA-Seq library preparation and sequencing. RiboTag RNA samples were sent to the Gladstone Institutes Genomics Core for quality control using Bioanalyzer (Agilent) and cDNA library preparation. cDNA was prepared with the Ovation RNA-Seq System V2 Kit (NuGEN, 7102), which uses a proprietary combination of enzymes and primers to preferentially prime non-rRNA sequences. First-strand cDNA synthesis is achieved with random hexamer primers and chimeric poly(T) primers, which bind to the region spanning the end of the 3'-UTR and the start of the poly(A) tail. Because stable mRNAs have at least 20 adenosine residues, the use of these chimeric poly(T) primers allows for preferential priming of adenylated messages (mRNAs) with minimal bias for messages with longer poly(A) tails. RNA-Seq libraries were constructed using the Ovation Ultralow System V2 (NuGEN, 0344) and analyzed by Bioanalyzer, quantified by qPCR (Kapa Biosystems, KR0405), and sequenced using the HiSeq 4000 system (Illumina).

Sequence quality assessment and trimming. The quality of the raw sequence data was checked via FASTQC. The sequence files were then trimmed using tools in Trimmomatic 0.36⁶⁴. The following were removed: Illumina TruSeq3 single-ended adapter sequences, bases with a quality score <3 at the start and end of a read, bases that had an average quality per base of <15 calculated using a sliding window to average four bases, and any reads that were shorter than 36 bases. The reads were single-ended and qualities were ASCII characters equal to the Phred quality plus 33.

Mapping and counting reads. HiSat2⁶⁵ was used to build indexes from the Reference Consortium Mouse Build 38 (mm10) and to align sequence reads to the genome. The resulting .bam files were sorted and indexed with SAMtools⁶⁶. Count files for each group were created with HTSeq using the mouse GENCODE Gene set release M11. The input data were .bam files, the data were not from a strand-specific assay, and the feature type used was "gene".

Differential expression (DE) analysis. The Bioconductor packages edgeR⁶⁷ and limma⁶⁸ were used for statistical analyses. Only reads with greater or equal to 10 counts per million reads (CPM) in at least two samples were kept. Trimmed mean of M -values (TMM) normalization, which accounts for compositional differences among the libraries, was then performed on HA reads and input reads, separately. Using the raw counts, dispersion, and design matrix, the negative binomial generalized linear model was fitted for each gene. Finally, pairwise likelihood ratio tests for young versus old was conducted. Translational efficiency

was calculated by using the ratio of the amount of mRNA recovered in the RiboTag pellet (HA-IP) over the total mRNA present in the oocyte (Input).

Gene ontology (GO) analysis. Gene lists were uploaded to DAVID 6.8^{69,70} and processed with the Functional Annotation Tool.

RNA-IP

The appropriate volume (80 μ l per sample) of Dynabeads™ Protein G was washed twice in 250 μ l incomplete lysis buffer (iLB: 30 mM Tris-HCl pH 7.4, 150 mM KCl, 10 mM MgCl_2 , 0.5% v/v NP-40, 0.25 mM Na_3VO_4 and 10 mM β -glycerophosphate) on a rotor at 4°C for 5 min per wash. Two additional washes were performed with 250 μ l complete LB (cLB: iLB supplemented with 5 \times HALT protease inhibitor, 1 mM DTT, 80 U/ml RNaseOUT, 80 U/ml RNasin and 2 \times ribonucleoside vanadyl complex) on a rotor at 4°C for 5 min per wash. The final wash solution was removed, and the beads were eluted to the original volume with cLB. Two hundred wild-type GV oocytes were collected in 10 μ l 0.1% w/v PVP and 250 U RNaseOUT in 1 \times PBS, flash-frozen in liquid nitrogen, and stored at -80°C . To homogenize the cells, 300 μ l of cLB was added, samples were vortexed for 30 s, and then incubated on ice for 10 min. The homogenates were then centrifuged for 15 min 20,817 \times g at 4°C , and the supernatants were transferred to new tubes. In total, 30 μ l (10%) of each supernatant was saved in 250 μ l RLT buffer supplemented with 1 mM DTT as input samples and the remaining volume was equally divided into the CPEB1-IP and the IgG-IP (control). The volume of each sample was increased to 300 μ l with cLB, 4 μ l (4 μ g) of the appropriate antibody (1/75, anti-CPEB1: Abcam, ab73287 and control IgG: Millipore, 12-371) was added to each tube, and samples were incubated on a rotor for 4 h at 4°C . Thirty microliters of washed beads were then added to each tube and samples were incubated on a rotor overnight at 4°C . The beads of each sample were pelleted using a magnetic rack and washed 4 times on a rotor at 4°C with 750 μ l wash buffer (WB: 30 mM Tris-HCl pH 7.4, 200 mM KCl, 10 mM MgCl_2 , 0.5% v/v NP-40, 0.25 mM Na_3VO_4 , 10 mM β -glycerophosphate, 1 \times HALT protease inhibitor, 1 mM DTT, 1 M urea, 50 U/ml RNaseOUT, and 50 U/ml RNasin) for 10 min per wash. After each wash, the beads were pelleted and the WB removed. Samples were transferred to a clean tube, and 250 μ l RLT buffer supplemented with 1 mM DTT was added to each sample. Samples were vortexed for 30 s, the beads were pelleted and removed. RNA extraction was performed following the Qiagen Rneasy Plus Micro Kit protocol. Samples were eluted in 14 μ l of RNase-free water and used for downstream RT-qPCR analysis.

RNA extraction and real-time quantitative PCR (RT-PCR)

Extracted RNA was reverse-transcribed using the SuperScript™ III First-Strand Synthesis System with random hexamer or oligo dT primers (Invitrogen, 18080-051). Gene expression was measured using TaqMan™ Assays and Taqman™ Fast Advanced Master Mix (ThermoFisher, 4444557). TaqMan Assays used were as follows; *Actb* (Mm02619580_g1), *Ccnb1* (Mm03053893_gH), *Ccnb2* (Mm01171453_m1), *Cpeb1* (Mm01314928_m1), *Dppa3* (Mm01184198_g1), *Eif4a1* (Mm03807704_g1), *Gata4* (Mm00484689_m1), *Golph3* (Mm00499420_m1), *Il7* (Mm01295803_m1), *Nlrp5* (Mm01143609_m1), *Thumpd1* (Mm00524010_m1), *Tpx2* (Mm01245970_m1), *Sirt1* (Mm01168521_m1), *Sirt7* (Mm01248607_m1), *Rpl19* (Mm02601633_g1), and *Zp3* (Mm00442176_m1). Preliminary qPCRs were done to test mRNA levels not changed in GV and MII oocytes. Among the tested genes, *Actb* and *Eif4a1* were expressed at similar levels in GV and MII when random hexamers were used for RT priming, while *Dppa3* and *Rpl19* were stable when oligo(-dT) were used. Since no genes were found to be stable with both priming conditions, we used the geometric mean of the four best candidates for the two priming conditions, and no differences were observed in the Ct values for either the meiotic stage or the priming method ($N = 6$; paired,

one-way ANOVA). Therefore, in all the experiments using qPCR the geometric mean of *Actb*, *Eif4a1*, *Dppa3*, and *Rpl19* Ct was used for data normalization. Ten microliter reactions were run on the QuantStudio 6 Flex Real-time PCR System (Applied Biosystems). Gene expression was quantified via the 2^{-Ct} method, and statistical analysis was performed via GraphPad Prism 8.

Reporter mRNA preparation

The *Ccnb1*, *Ccnb2*, *Golph3*, *Il7*, *Nlrp5*, *Thumpd1*, and *Tpx2* 3'-UTR and *Cpeb1* open reading frame sequences (Supplementary Data 3) were obtained by amplification of mRNA from oocytes with appropriate primers (Supplementary Data 4). YFP reporters, mCherry, and FL reporters were subcloned in the pcDNA 3.1 vector and RL reporters were prepared in the pRL-TK vector, both containing a T7 promoter that allows in vitro transcription to synthesize mRNAs, and fidelity was confirmed by DNA sequencing. All reporters included a stretch of 20A at the 3' end. The mCherry reporter was in vitro polyadenylated and contained a poly(A) tail of 150–200 A. mRNA reporters were transcribed in vitro to synthesize mRNAs with mMESSAGE mMACHINE T7 Transcription Kit (Ambion, AM1344); polyadenylation of mCherry and Firefly luciferase was obtained using Poly(A) Tailing Kit (Ambion, AM1350). All the messages were purified using MEGAclear Kit (Ambion, AM1908). mRNA concentrations were measured by NanoDrop, and its integrity was evaluated by electrophoresis.

Luciferase assay

Oocytes still enclosed in the cumulus cells (CEOs) were injected with 12.5 ng/ μ l *Il7-RL*, *Thumpd1-RL*, or *Tpx2-RL* and 12.5 ng/ μ l of polyadenylated FL using a FemtoJet Express programmable microinjector with an Automated Upright Microscope System (Leica, DM4000B). Injected CEOs were pre-incubated for 3 h in culture medium supplemented with 2 μ M milrinone, and then cultured in milrinone-free medium supplemented with 100 nM amphiregulin. After 16 h, the CEOs were denuded, collected in lysis buffer and frozen. Luciferase activities in the oocyte extracts were measured using a dual-luciferase reporter assay kit (Promega), and luminescence was detected with a SpectraMax L luminometer (Molecular Devices). Data are reported as ratios of RL and FL.

YFP reporter assay

Ccnb1-YFP, *Ccnb2-YFP*, *Il7-YFP*, *Golph3-YFP*, *Thumpd1-YFP*, or *Tpx2-YFP* were injected in oocytes at 12.5 ng/ μ l with polyadenylated *mCherry* at 12.5 μ g/ μ l using a FemtoJet Express programmable microinjector with an Automated Upright Microscope System. After pre-incubating 3 h or overnight in α -MEM medium with 1 μ M cilostamide, oocytes were released in cilostamide-free medium for in vitro maturation or incubated with cilostamide to maintain GV state. Time-lapse recordings were performed using a Nikon Eclipse T2000-E equipped with a mobile stage and environmental chamber of 37 °C and 5% CO₂ at the following settings: filter set, dichroic mirror YFP/CFP/mCherry 69008BS; Ypet channel (Ex: S500/20 \times 49057 Em: D535/30 m 47281); and mCherry channel (Ex: 580/25 \times 49829 Em: 632/60 m). Images were processed and fluorescence was quantified using MetaMorph (Molecular Devices). Ratios of YFP reporter of the plateaued level of mCherry signal were reported as the protein accumulation during oocyte maturation. The rate of translation were calculated with YFP/mCherry ratios as the slope of the simple linear regression curve at the indicated time interval.

In vitro CDK1 kinase assay

Oocytes were collected in 30 μ l of 2 \times kinase buffer (100 mM HEPES, 30 mM MgCl₂, 2 mM EGTA, 10 mM CaCl₂, 2 mM DTT, 2 μ g/ml leupeptin, 2 μ g/ml aprotinin, 2 μ M okadaic acid). Oocytes were lysed by freezing and thawing twice in liquid nitrogen. Extracts were incubated at 30 °C for 30 min in the presence of 0.1 mM ATP, 10 mM DTT, 2 μ M

okadaic acid, and 2 μ g of recombinant peptide GST-PP1 as the substrate. PP1-GST was produced as previously described⁴⁷. Reactions were stopped by adding Laemmli sample buffer and boiling at 95 °C for 5 min. CDK1 activity was measured by quantifying the western blot signal of phosphorylated T320 of the total substrate loaded evaluated by Ponceau S staining.

Western blotting

Oocytes were lysed in 10 μ l of 0.1% w/v PBS/PVP with 4 μ l Laemmli buffer (Bio-Rad, 161-0747) with β -mercaptoethanol (Gibco 21985023), a phosphatase inhibitor, and protease inhibitor. The oocyte lysates were boiled for 5 min at 95 °C and left on ice, then separated on 10% v/v or 12% v/v polyacrylamide gels and transferred to a Polyvinylidene difluoride (PVDF) membrane (Millipore ISEQ00010). Membranes were blocked in 5% w/v milk for 1 h at room temperature and incubated with primary antibody overnight at 4 °C. The primary antibody and dilutions used were as follows: CPEB1 (Abcam, ab73287, 1:1000), α -tubulin (Sigma-Aldrich, T6074, 1:10,000), T320-pp1 (Abcam, ab62334, 1:30,000). Membranes were washed in TBS-Tween 20 (0.05% v/v) and incubated with HRP-conjugated secondary antibodies, 1:10,000 anti-rabbit IgG (GE Healthcare, NA934V) and 1:10,000 anti-mouse IgG (GE Healthcare NA931V), for 2 h at room temperature. Signals were detected using Clarity Western ECL substrate (Bio-Rad, 170-5061). The images are analyzed with the ImageJ 1.53a.

Statistical analysis

Statistical analysis was performed using the GraphPad Prism 9.3.1 package. The statistical analysis performed depended on a specific experiment and is described within the figure legend. For comparison between two groups, a two-tailed paired or unpaired *t* test was used, for multiple comparison, one-way ANOVA was used. Statistical significance is denoted by an asterisk in each graph. The quality of RNA-Seq reads were performed using FastQC and reads were then trimmed with Trimmomatic 0.36. Alignment of the reads to the mouse genome was performed by Hisat2, .bam files were sorted and indexed using Samtools, and count files were generated by HTSeq. TMM normalization and the remaining RNA-Seq statistical analyses were done through edgeR.

Reporting summary

Further information on research design is available in the Nature Portfolio Reporting Summary linked to this article.

Data availability

RiboTag-IP/RNA-Seq data have been deposited in the NCBI Gene Expression Omnibus (GEO) database under the accession code GSE222638. The published available datasets used in this work were from NCBI Gene Expression Omnibus (GEO) accession number GDS3295 [<https://www.ncbi.nlm.nih.gov/geo/query/acc.cgi?acc=GSE11667>] (Aging transcriptome²⁴), GSE35106 (Polysome array¹⁴), GSE135525 (RiboTag IP/RNA-Seq¹⁵), GSE165782 (PAI-seq⁷¹), and GRCm38 [https://www.ncbi.nlm.nih.gov/assembly/GCF_000001635.20] (mouse genome dataset). The data supporting the findings of this study are available from the corresponding authors upon reasonable request. Source data are provided with this paper.

References

1. Fedarko, N. S. The biology of aging and frailty. *Clin. Geriatr. Med.* **27**, 27–37 (2011).
2. Klein, J. & Sauer, M. V. Assessing fertility in women of advanced reproductive age. *Am. J. Obstet. Gynecol.* **185**, 758–770 (2001).
3. Navot, D. et al. Poor oocyte quality rather than implantation failure as a cause of age-related decline in female fertility. *Lancet* **337**, 1375–1377 (1991).
4. Sauer, M. V. The impact of age on reproductive potential: lessons learned from oocyte donation. *Maturitas* **30**, 221–225 (1998).

5. Jones, K. T. & Lane, S. I. Molecular causes of aneuploidy in mammalian eggs. *Development* **140**, 3719–3730 (2013).
6. Hassold, T. & Hunt, P. Maternal age and chromosomally abnormal pregnancies: what we know and what we wish we knew. *Curr. Opin. Pediatr.* **21**, 703–708 (2009).
7. Titus, S., Stobezki, R. & Oktay, K. Impaired DNA repair as a mechanism for oocyte aging: is it epigenetically determined? *Semin Reprod. Med.* **33**, 384–388 (2015).
8. Gosden, R. & Lee, B. Portrait of an oocyte: our obscure origin. *J. Clin. Invest.* **120**, 973–983 (2010).
9. Eppig, J. J. Coordination of nuclear and cytoplasmic oocyte maturation in eutherian mammals. *Reprod. Fertil. Dev.* **8**, 485–489 (1996).
10. Combelles, C. M., Cekleniak, N. A., Racowsky, C. & Albertini, D. F. Assessment of nuclear and cytoplasmic maturation in in-vitro matured human oocytes. *Hum. Reprod.* **17**, 1006–1016 (2002).
11. Li, R. & Albertini, D. F. The road to maturation: somatic cell interaction and self-organization of the mammalian oocyte. *Nat. Rev. Mol. Cell Biol.* **14**, 141–152 (2013).
12. Bianchi, S. et al. Ultrastructural markers of quality are impaired in human metaphase II aged oocytes: a comparison between reproductive and in vitro aging. *J. Assist Reprod. Genet.* **32**, 1343–1358 (2015).
13. Clarke, H. J. Post-transcriptional control of gene expression during mouse oogenesis. *Results Probl. Cell Differ.* **55**, 1–21 (2012).
14. Chen, J. et al. Genome-wide analysis of translation reveals a critical role for deleted in azoospermia-like (Dazl) at the oocyte-to-zygote transition. *Genes Dev.* **25**, 755–766 (2011).
15. Luong, X. G., Daldello, E. M., Rajkovic, G., Yang, C. R. & Conti, M. Genome-wide analysis reveals a switch in the translational program upon oocyte meiotic resumption. *Nucleic Acids Res.* **48**, 3257–3276 (2020).
16. Yartseva, V. & Giraldez, A. J. The Maternal-to-zygotic transition during vertebrate development: a model for reprogramming. *Curr. Top. Dev. Biol.* **113**, 191–232 (2015).
17. Chen, J. et al. Somatic cells regulate maternal mRNA translation and developmental competence of mouse oocytes. *Nat. Cell Biol.* **15**, 1415–1423 (2013).
18. Franciosi, F., Manandhar, S. & Conti, M. FSH regulates mRNA translation in mouse oocytes and promotes developmental competence. *Endocrinology* **157**, 872–882 (2016).
19. Conti, M. & Franciosi, F. Acquisition of oocyte competence to develop as an embryo: integrated nuclear and cytoplasmic events. *Hum. Reprod. Update* **24**, 245–266 (2018).
20. Richter, J. D. CPEB: a life in translation. *Trends Biochem Sci.* **32**, 279–285 (2007).
21. Pique, M., Lopez, J. M., Foissac, S., Guigo, R. & Mendez, R. A combinatorial code for CPE-mediated translational control. *Cell* **132**, 434–448 (2008).
22. Grondahl, M. L. et al. Gene expression profiles of single human mature oocytes in relation to age. *Hum. Reprod.* **25**, 957–968 (2010).
23. Hamatani, T. et al. Age-associated alteration of gene expression patterns in mouse oocytes. *Hum. Mol. Genet.* **13**, 2263–2278 (2004).
24. Pan, H., Ma, P., Zhu, W. & Schultz, R. M. Age-associated increase in aneuploidy and changes in gene expression in mouse eggs. *Dev. Biol.* **316**, 397–407 (2008).
25. Steuerwald, N. M., Bermudez, M. G., Wells, D., Munne, S. & Cohen, J. Maternal age-related differential global expression profiles observed in human oocytes. *Reprod. Biomed. Online* **14**, 700–708 (2007).
26. de Vantery, C., Stutz, A., Vassalli, J. D. & Schorderet-Slatkine, S. Acquisition of meiotic competence in growing mouse oocytes is controlled at both translational and posttranslational levels. *Dev. Biol.* **187**, 43–54 (1997).
27. Del Llano, E. et al. Age-related differences in the translational landscape of mammalian oocytes. *Aging Cell* **19**, e13231 (2020).
28. Sanz, E. et al. Cell-type-specific isolation of ribosome-associated mRNA from complex tissues. *Proc. Natl Acad. Sci. USA* **106**, 13939–13944 (2009).
29. Sousa Martins, J. P. et al. DAZL and CPEB1 regulate mRNA translation synergistically during oocyte maturation. *J. Cell Sci.* **129**, 1271–1282 (2016).
30. Sha, Q. Q. et al. Dynamics and clinical relevance of maternal mRNA clearance during the oocyte-to-embryo transition in humans. *Nat. Commun.* **11**, 4917 (2020).
31. Zhang, C., Wang, M., Li, Y. & Zhang, Y. Profiling and functional characterization of maternal mRNA translation during mouse maternal-to-zygotic transition. *Sci. Adv.* **8**, eabj3967 (2022).
32. Hu, W. et al. Single-cell transcriptome and translational dual-omics reveals potential mechanisms of human oocyte maturation. *Nat. Commun.* **13**, 5114 (2022).
33. Tharakan, R., Ubaida-Mohien, C., Piao, Y., Gorospe, M. & Ferrucci, L. Ribosome profiling analysis of human skeletal muscle identifies reduced translation of mitochondrial proteins with age. *RNA Biol.* **18**, 1555–1559 (2021).
34. Anisimova, A. S. et al. Multifaceted deregulation of gene expression and protein synthesis with age. *Proc. Natl Acad. Sci. USA* **117**, 15581–15590 (2020).
35. van Heesch, S. et al. The translational landscape of the human heart. *Cell* **178**, 242–260 e229 (2019).
36. Jang, J. Y., Blum, A., Liu, J. & Finkel, T. The role of mitochondria in aging. *J. Clin. Invest.* **128**, 3662–3670 (2018).
37. van der Reest, J., Nardini Cecchino, G., Haigis, M. C. & Kordowitzki, P. Mitochondria: their relevance during oocyte ageing. *Ageing Res Rev.* **70**, 101378 (2021).
38. Li, L., Baibakov, B. & Dean, J. A subcortical maternal complex essential for preimplantation mouse embryogenesis. *Dev. Cell* **15**, 416–425 (2008).
39. Racedo, S. E., Rawe, V. Y. & Niemann, H. Dynamic changes of the Golgi apparatus during bovine in vitro oocyte maturation. *Reproduction* **143**, 439–447 (2012).
40. Sas-Chen, A. et al. Dynamic RNA acetylation revealed by quantitative cross-evolutionary mapping. *Nature* **583**, 638–643 (2020).
41. Cakmak, H., Franciosi, F., Zamah, A. M., Cedars, M. I. & Conti, M. Dynamic secretion during meiotic reentry integrates the function of the oocyte and cumulus cells. *Proc. Natl Acad. Sci. USA* **113**, 2424–2429 (2016).
42. Costermans, N. G. J., Daldello, E. M., Marathe, R. J. & Conti, M. Defining the program of maternal mRNA translation during in vitro maturation using a single oocyte reporter assay. *J. Vis. Exp.* **172**, e62041 (2021).
43. Yu, C. et al. BTG4 is a meiotic cell cycle-coupled maternal-zygotic-transition licensing factor in oocytes. *Nat. Struct. Mol. Biol.* **23**, 387–394 (2016).
44. Ingolia, N. T., Ghaemmghami, S., Newman, J. R. & Weissman, J. S. Genome-wide analysis in vivo of translation with nucleotide resolution using ribosome profiling. *Science* **324**, 218–223 (2009).
45. Han, S. J. et al. The translation of cyclin B1 and B2 is differentially regulated during mouse oocyte reentry into the meiotic cell cycle. *Sci. Rep.* **7**, 14077 (2017).
46. Daldello, E. M., Luong, X. G., Yang, C. R., Kuhn, J. & Conti, M. Cyclin B2 is required for progression through meiosis in mouse oocytes. *Development* **146**, dev172734 (2019).
47. Daldello, E. M. et al. Control of Cdc6 accumulation by Cdk1 and MAPK is essential for completion of oocyte meiotic divisions in *Xenopus*. *J. Cell Sci.* **128**, 2482–2496 (2015).
48. Lewis, C. W. et al. A western blot assay to measure cyclin dependent kinase activity in cells or in vitro without the use of radioisotopes. *FEBS Lett.* **587**, 3089–3095 (2013).

49. Racki, W. J. & Richter, J. D. CPEB controls oocyte growth and follicle development in the mouse. *Development* **133**, 4527–4537 (2006).
50. Sha, Q. Q. et al. A MAPK cascade couples maternal mRNA translation and degradation to meiotic cell cycle progression in mouse oocytes. *Development* **144**, 452–463 (2017).
51. Duncan, F. E., Chiang, T., Schultz, R. M. & Lampson, M. A. Evidence that a defective spindle assembly checkpoint is not the primary cause of maternal age-associated aneuploidy in mouse eggs. *Biol. Reprod.* **81**, 768–776 (2009).
52. Yamamoto, T. et al. Effect of maternal age on the developmental competence and progression of nuclear maturation in bovine oocytes. *Mol. Reprod. Dev.* **77**, 595–604 (2010).
53. Koncicka, M. et al. Increased expression of maturation promoting factor components speeds up meiosis in oocytes from aged females. *Int. J. Mol. Sci.* **19**, 2841 (2018).
54. Davydenko, O., Schultz, R. M. & Lampson, M. A. Increased CDK1 activity determines the timing of kinetochore-microtubule attachments in meiosis I. *J. Cell Biol.* **202**, 221–229 (2013).
55. Dong, F. et al. Inhibition of CDK4/6 kinases causes production of aneuploid oocytes by inactivating the spindle assembly checkpoint and accelerating first meiotic progression. *Biochim Biophys. Acta Mol. Cell Res.* **1868**, 119044 (2021).
56. Lane, S. I., Chang, H. Y., Jennings, P. C. & Jones, K. T. The Aurora kinase inhibitor ZM447439 accelerates first meiosis in mouse oocytes by overriding the spindle assembly checkpoint. *Reproduction* **140**, 521–530 (2010).
57. Dai, X. X. et al. A combinatorial code for mRNA 3'-UTR-mediated translational control in the mouse oocyte. *Nucleic Acids Res.* **47**, 328–340 (2019).
58. Oe, S. et al. Cpeb1 expression is post-transcriptionally regulated by AUF1, CPEB1, and microRNAs. *FEBS Open Bio* **12**, 82–94 (2022).
59. Bestetti, I. et al. High-resolution array-CGH analysis on 46,XX patients affected by early onset primary ovarian insufficiency discloses new genes involved in ovarian function. *Hum. Reprod.* **34**, 574–583 (2019).
60. Hyon, C. et al. Deletion of CPEB1 gene: a rare but recurrent cause of premature ovarian insufficiency. *J. Clin. Endocrinol. Metab.* **101**, 2099–2104 (2016).
61. McGuire, M. M. et al. Genomic analysis using high-resolution single-nucleotide polymorphism arrays reveals novel microdeletions associated with premature ovarian failure. *Fertil. Steril.* **95**, 1595–1600 (2011).
62. Tsuiko, O. et al. Copy number variation analysis detects novel candidate genes involved in follicular growth and oocyte maturation in a cohort of premature ovarian failure cases. *Hum. Reprod.* **31**, 1913–1925 (2016).
63. Calderone, V. et al. Sequential functions of CPEB1 and CPEB4 regulate pathologic expression of vascular endothelial growth factor and angiogenesis in chronic liver disease. *Gastroenterology* **150**, 982–997 e930 (2016).
64. Bolger, A. M., Lohse, M. & Usadel, B. Trimmomatic: a flexible trimmer for Illumina sequence data. *Bioinformatics* **30**, 2114–2120 (2014).
65. Kim, D., Langmead, B. & Salzberg, S. L. HISAT: a fast spliced aligner with low memory requirements. *Nat. Methods* **12**, 357–360 (2015).
66. Li, H. et al. The sequence Alignment/Map format and SAMtools. *Bioinformatics* **25**, 2078–2079 (2009).
67. Robinson, M. D., McCarthy, D. J. & Smyth, G. K. edgeR: a Bioconductor package for differential expression analysis of digital gene expression data. *Bioinformatics* **26**, 139–140 (2010).
68. Ritchie, M. E. et al. limma powers differential expression analyses for RNA-sequencing and microarray studies. *Nucleic Acids Res.* **43**, e47 (2015).
69. Huang da, W., Sherman, B. T. & Lempicki, R. A. Systematic and integrative analysis of large gene lists using DAVID bioinformatics resources. *Nat. Protoc.* **4**, 44–57 (2009).
70. Huang da, W., Sherman, B. T. & Lempicki, R. A. Bioinformatics enrichment tools: paths toward the comprehensive functional analysis of large gene lists. *Nucleic Acids Res.* **37**, 1–13 (2009).
71. Xiong, Z. et al. Ultrasensitive Ribo-seq reveals translational landscapes during mammalian oocyte-to-embryo transition and pre-implantation development. *Nat. Cell Biol.* **24**, 968–980 (2022).

Acknowledgements

We thank Dr. Raúl Méndez and Dr. Gonzalo Fernandez-Miranda (The Barcelona Institute of Science and Technology) for sharing the CPEB1-targeted mice, and Dr. Chisato Kunitomi and Hong Kung Li for sample collection. This work was supported by NIH/NICHD P50 HD055764 Center for Research and Innovation and Training in Reproduction and Infertility, the NIH R01 GM116926. This project was funded in part by grant number GCRLE-1020 from the Global Consortium for Reproductive Longevity and Equality at the Buck Institute, made possible by the Bia-Echo Foundation. The authors acknowledge the support of the UCSF Bakar Aging Research Institute for the purchase of aged mice, and Drs. Leanne Jones and Saul Villeda for the helpful discussion.

Author contributions

M.C. designed the study. N.T., F.F., E.M.D., X.G.L., P.A., and X.W. performed experiments. N.T. and M.C. analyzed data. N.T. and M.C. wrote the first draft of the paper and all the authors contributed to its revision.

Competing interests

The authors declare no competing interests.

Additional information

Supplementary information The online version contains supplementary material available at <https://doi.org/10.1038/s41467-023-35994-3>.

Correspondence and requests for materials should be addressed to Marco Conti.

Peer review information *Nature Communications* thanks Mirko Völkers and the other, anonymous, reviewers for their contribution to the peer review of this work.

Reprints and permissions information is available at <http://www.nature.com/reprints>

Publisher's note Springer Nature remains neutral with regard to jurisdictional claims in published maps and institutional affiliations.

Open Access This article is licensed under a Creative Commons Attribution 4.0 International License, which permits use, sharing, adaptation, distribution and reproduction in any medium or format, as long as you give appropriate credit to the original author(s) and the source, provide a link to the Creative Commons license, and indicate if changes were made. The images or other third party material in this article are included in the article's Creative Commons license, unless indicated otherwise in a credit line to the material. If material is not included in the article's Creative Commons license and your intended use is not permitted by statutory regulation or exceeds the permitted use, you will need to obtain permission directly from the copyright holder. To view a copy of this license, visit <http://creativecommons.org/licenses/by/4.0/>.

© The Author(s) 2023, corrected publication 2023